Comparative Views of Major Regions of Active Normal Fault-Bounded Basins and Crustal Extension on Earth

Steven G. Wesnousky
Center for Neotectonic Studies and
Nevada Seismological Laboratory
Mail Stop 174
1664 North Virginia Street
University of Nevada, Reno
Reno, Nevada 89557
email: wesnousky@unr.edu

Abstract

To provide a comparative study that considers all of the major regions of active crustal extension motivates effort here to provide graphical views of the geological, geophysical and tectonic characteristics of the Apennines of Italy, the Tibetan Plateau, the Aegean Sea and adjacent areas of Greece and Turkey, the Basin and Range in western North America, the Ordos and Baikal regions in northwest Asia, the East African Rift, and areas along the Japan Trench and the Mid-Atlantic Ridge. The views offer insight to the factors that control basin development and systematic variations in basin size that exist between the regions.

Introduction

Sedimentary basins bounded by active normal fault-bounded range fronts distinguish the Basin and Range province of North America. The physiography and structure result from active crustal extension. Provinces of crustal extension likewise exist within and along the margins of the Aegean Sea, Africa, the Siberia and Mongolia regions of Eurasia, the Himalaya of Tibet, and within the oceans along portions of the ridges and trenches that define plate boundaries **(Figure 1)**. Papers describing the tectonics of each region are too many to cite. Discussion sections in these papers, and even entire papers (e.g., Pavlovsky, 1948; Logatchev et al., 1983; Cemen, 2010), often place a focus on comparing features observed in one area of extension to another that is viewed to share a like genesis. The seeming absence of a comparative study that considers all of the major regions of active crustal extension motivates effort here to provide a graphical view of the geological and geophysical characteristics that are shared and distinctive among the regions.

Physiographic maps of the regions outlined in **Figure 1** are presented in **Figures 2**. The normal fault-bounded basins are generally manifest by the presence of smooth alluvial or lake-filled basins sharply bounded by higher and more rugged topography of adjacent mountains. **Tables 1 to 9** list and provide explanation to the sources and manners of measurement of geological and geophysical parameters that are representative of the respective basins and regions of their location. Each basin in **Tables 1 to 9** is assigned a *map number* and there the respective basin names are listed. The *map number* corresponds to the number allocated to each basin in the respective areas of **Figures 2**. Individual basins are also assigned a unique *plot number* designed to aid in comparatively viewing the observations for each region. For example, the surface areas of each basin are plotted in **Figure 3** as a function of plot number. The measurements for each region are arranged such that the 7 continental regions appear on the left of the plot followed by the two submarine regions on the right. It is this type of plot in the subsequent sections that provides a primary means of comparatively viewing and discussing the geological and geophysical characteristics of each region. Ensuing plots are designed to provide perspective on the factors responsible for the distinct regional differences in basin sizes shown in **Figure 3**.

Narratives of the (1) geographic and historical context relating to current understanding of tectonics, (2) the physiographic and structural character of fault-bounded basins, (3) the distribution and age of volcanism, (4) temporal bounds on when rifting commenced, (5) observations of heat-flow, (6) the depth of seismicity, (7) crustal structure, and (8) geodetic rates of deformation provide additional reference to the information organized **Tables 1 to 9.** The regional narratives are largely the result of literature review, allocated to the **Appendix,** and left to the reader to consider later in context of the plots that summarize the information and subsequent discussion.

Comparative Views

Elevation and Topography

The elevations of basin floors and highest adjacent mountain peaks are given in **Figures 4a** and **b**. The average of the two measures in shown in **Figure 4c**. The average values in the continental regions range from 0 to 6000 m, excepting those in the Aegean Sea which are submarine. The crust of the submarine Aegean Sea is generally interpreted to be highly extended continental crust and, though not typical continental crust, is here grouped with the continental values. In contrast to the continental regions, average basin elevations group around 3000 m to 7000 m below sea level along the Mid-Atlantic ridge and Japan trench, respectively. The presence of major extensional environments spanning from the deepest depths of the oceans to the highest of mountains **(Figure 4)** precludes absolute elevation as a primary factor in controlling the regional distribution of active normal fault-bounded basins.

Topographic relief across all basins is displayed in **Figure 4d**, estimated as the difference in basin elevations (**Figure 4a**) and the elevations of the highest adjacent peaks (**Figure 4b**). Topographic relief of basins most frequently falls between ~500 and ~2000 m, with the exception of the Japan Trench and the Mid-Atlantic that exhibit values of relief that cluster at the upper and lower limits of those observed on the continents.

Spatial Dimensions

Normal fault-bounded basins are generally elongated in the direction of the main bounding active fault(s). It is this that allows a reasonable first-order description of their dimensions in terms of an average length and width. The lengths and widths of all basins are the subject of **Figures 5a and b.** The spatial area encompassed by each basin is derived by multiplying the respective lengths and widths and plotted in **Figure 5c**. The arrangement of values by plot number is such that differences in observed ranges of length, width, and area for the separate continental regions increase from left to right across the plot. The range of continental basin sizes extends over several orders of magnitude, such that there is virtually no overlap between those areas exhibiting the largest and smallest basins (e.g. Italy and Tibet versus Baikal and Africa). The areas of the Japan Trench and Mid-Atlantic basins, while plotted separately, follow the approximate trend observed for continents. The ratio of basin lengths between the Mid-Atlantic and Japan Trench (**Figure 5a**) is distinctly less than the ratio of basin widths (**Figure 5b**) for the same two regions. Such disparity is not apparent for any of the continental areas.

Dividing basin lengths by their respective widths yields the measures of aspect ratio plotted in **Figure 6a**. Aspect ratios of basins in all regions of extension are most frequently between 2 and 10, with median values of between about 3 and 5 within the continental regions and a larger 6 to 8 in the two marine areas. Basin lengths are plotted directly versus basin widths in **Figure 6b**. A linear regression through the observations points to an average aspect ratio across all basins equal to 4.5. A similar aspect ratio of 4.3 is estimated when only continental basins are considered in absence of the two oceanic regions in **Figure 6c**. Linear regressions limited to the marine Mid-Atlantic and Japan trench regions yield larger aspect ratios of 8 and greater **(Figure 6d)**. Basins in the two marine areas thus tend be longer and skinnier than the majority of continental basins.

Additionally plotted in **Figure 6c** are linear regressions limited to basins in the separate continental regions. Slopes and thus best fitting aspect ratios vary from 2.3 to 5.1, with the limiting values occurring respectively for the regions displaying the smallest and largest basin areas, specifically Italy and Africa, allowing the suggestion that aspect ratio may exhibit a tendency to increase with basin size. The same is hinted at by the apparent increase in the lower limits of aspect ratios observed in **Figure 6a**, where the continental regions are arranged from left to right in increasing order of average basin size.

The fit of a logarithmic relationship in **Figure 7a** between aspect ratios and basin sizes in all of the extensional regions illustrates the tendency for aspect ratios to increase with basin area, albeit with much scatter. The data for the two marine areas are considered separately in **Figures 7b**. Aspect ratios visibly increase with basin size for basins along the Japan Trench and Mid-Atlantic ridge (**Figure 7b**). If considered to reflect a singular model of basin growth, the data might be interpreted to reflect that marine basin growth is preferentially accommodated by increases in basin length as compared to width.

Aspect ratio versus basin area is plotted for basins only the continental regions in **Figure 7c**, and the apparent tendency for aspect ratio to increase with basin area is much less than observed in **Figure 7b** for the marine areas. The regression fit through the data describes a nearly one unit increase in aspect ratio for each 10 fold increase in area. The result is similar when only median values are plotted (**Figure 7d**), but with the notable outlier of relatively long basins that occur in Turkey. As with the marine areas, it might be considered that the tendency for aspect ratio to increase with basin size reflects a continuum whereby basin growth is accommodated by progressively greater increases in basin length as compared to width. The suggestion is complicated by the previously noted observations of **Figure 5c** that suggest the regional variations in basin sizes are possibly the result of geophysical and tectonic characteristics unique to the respective regions. In this sense, the tendency for aspect ratio to increase with basin area may not reflect a universal character of basin growth but rather the geophysical and tectonic characteristics of the regions displaying the differing ranges of basin sizes. As well, examination of plots constructed for the individual continental areas in **Figures 7 e thru f** do not indicate increases in aspect ratio with basin size. The reason behind the apparent increase in continental basin aspect ratios with basin size is thus uncertain.

Basin Fill and Structural Relief (versus Basin Area and Basin Length)

Basin fill thicknesses are plotted in **Figure 8a**. The reported values are largely from seismic reflection and refraction surveys with the exception of those in Nevada where measures are derived from gravity models. Instances of fill thickness greater than ~7000 m are recorded in Africa, Baikal, the Basin and Range, and the Ordos. Maximum fill values are less in the Aegean, and least in Italy. Reports indicate virtually no post-graben sedimentation in the two oceanic regions, and observations appear largely absent for Tibet.

Adding the basin fill thicknesses of **Figure 8a** to respective measures of topographic relief in **Figure 4d** provides the estimates of *structural relief* across each basin that are depicted in **Figure 8b.** Maximal values of 10,000 m or more are registered in Africa, Baikal, and the Ordos. In contrast, values in Italy never surpass 3000 m and are mostly less than 1500m. Information for basin fill deposit thicknesses in Tibet appear largely absent and so values for the region are only a lower bound. Values of structural relief for the continental areas show a general increase from left to right across the plot of **Figure 8b**. As arranged, the increase reflects a commensurate increase in average basin sizes. The relationship is further illustrated in **Figure 8c** where basin areas are plotted versus respective values of structural relief. The observations in total may be described with a power law distribution. The values for each extensional region are though located in distinctly different areas of the plot and, when fit to power law distributions, individual areas exhibit different and lesser exponents of growth than the overall data. As with discussion of the relationship of aspect ratio to basin area that accompanied **Figure 7**, caution might be placed in assuming the observed overall trend reflects a simple

model of basin growth. Other geophysical and tectonic factors unique to the different regions are likely playing a role.

The observed structural reliefs of basins in the two marine areas as plotted in **Figures 8b and d** are limited to less than ~500 m along the Japan trench and mostly between 2000 and 3000 m along the Mid-Atlantic ridge. Basin area shows little to no increase with structural relief along the Japan trench whereas basin area appears to increase rapidly with respect to structural relief along the Mid-Atlantic, though the range of structural relief is quite small for this latter assessment. The structural relief values of basins along the Japan trench are unique in there relatively small sizes.

Basin structural reliefs are further plotted versus respective basin lengths in **Figure 9a**. Immediately apparent are the basins of the Japan Trench which fall well below the alignment of values formed by the remaining extensional areas. Attention is limited to the continental regions of extension in **Figure 9b**. Here the sum of observations is described by a power law distribution. The result is not surprising in the sense that the relationship between fault length and fault displacement has been shown to satisfy a power law distribution (Dawers et al., 1993; Scholz et al., 1993; Lathrop et al., 2022), and in a first order manner structural relief and basin length are proxies for total displacement and the length of basin bounding faults. The fields of values describing the two marine areas are viewed separately as in **Figure 9c**. They each exhibit slopes distinct from the overall trend of the continental basins. The flat arrangement of the Mid-Atlantic points suggests structural relief largely independent of basin length whereas the vertical arrangement of Japan Trench measures suggests basin lengths are largely independent of structural relief.

The ratio of basin fill depth to topographic relief in each basin is portrayed in **Figure 9d**. Basin fill tends to be a greater contribution to structural relief (ratios >1) in about 30% and 80% of basins on the continents, with the exception of Italy where topography is in virtually all basins the primary contributor to structural relief (ratios <1). An absence of sedimentary fill within the Japan trench and Mid-Atlantic basins leads to ratios of zero for the two marine areas.

Geophysical Characteristics

Moho depths are plotted versus plot number **Figures 10a**. Moho depths are observed beneath the continental basins of the Ordos, Baikal, and Africa to be on the order of 40 km, less than 30 km beneath those of Italy, and intermediate to those values beneath portions of the Aegean and Basin and Range. Recalling **Figure 5c**, the distribution of values in **Figure 10a** suggests continental basin areas tend to be larger where Moho depths are larger, with Tibet being a glaring exception to the trend with its extremely deep Moho of 70-80 km. These observations are emphasized in **Figure 10b** where basin areas are plotted directly versus Moho depths. Values for Tibet fall well off the observed tendency of basins in the other continental areas to increase with Moho depth. In this regard, Tibet emphasizes that factors other than crustal structure are contributing to the variations of basin sizes observed across the continental regions. This is underscored by large differences in basin areas that exists between the Japan Trench and Mid-Atlantic extensional regions, each of which are developed on crust exhibiting similar and shallow Moho depths (**Figure 10b**). As well, Moho depths are significantly less beneath the oceanic areas than those in the continents.

Seismogenic depths beneath the extensional regions are plotted in **Figure 10c**. Values beneath individual regions of extension range from < 10 to ~ 40 km. Apparent is an imperfect tendency for basins sizes in the continental areas to increase with seismogenic thickness, without any major exceptions like that displayed by Tibet when considering Moho depths in **Figure 10a**. The tendency is further emphasized in **Figure 10d** with the direct plotting of basin areas versus seismogenic depth. Given that the basins are the result of earthquake fault displacements, such a correlation may be expected. The marine areas offer a stark contrast: the small basins of the Japan trench (**Figure 5c**) are associated with a much deeper seismogenic layer than observed beneath the larger basins of the Mid-Atlantic Ridge (**Figure 5c**). Here other factors rather than displacement

on basin bounding faults must play a role in controlling the depth of seismicity in the regions, particularly along the Japan Trench.

Heat Flow values range between ~25 to 120 MWm^{-2} across continental regions (**Figure 11**). The significance of differences between areas should be questioned because the number of direct measurements vary and are often few across regions. Likewise the variation in individual measurements across regions is typically large, and modulated by effects of hydrothermal fluid flow. Any suggestion of a simple relationship between observed basin sizes and heat flow is lacking in **Figure 11**.

Earthquake Size. The largest instrumentally recorded normal fault earthquakes accompanied by estimates of Mw are mostly limited to between Mw 7 and 7.5 on the continents (**Figure 12**), but for the larger Mw 7.7 1956 Amorgos earthquake within the Aegean Sea. Among all the extensional regions, only along the Japan Trench have Mw 8 earthquakes been reported. Italy is distinguished by a lack of any instrumentally recorded earthquakes of Mw 7 or greater and earthquakes along the Mid-Atlantic ridge generally don't surpass Mw 6.

Histories of Deformation and Volcanism.

Initiation Ages of basins (**Figures 13a**) are derived from a mixed data set. In various regions like the Aegean, Africa, Baikal, and the Ordos values are derived from the estimated ages of the deepest basin fill on basement, whereas in others the values are derived from tectonic arguments. The current regimes of extension around the planet have largely initiated in the last 20 my with the exception of subsets of basins in the Aegean, the Ordos, and Baikal where initiation ages of some basins are possibly double this value. The youngest initiation ages of a few million years or less are found in Italy, the Japan Trench, and Mid-Atlantic ridge. A systematic increase in basin size with initiation age is not clearly evident in either the continental or marine regions (**Figure 13b**), though the largest basins in the Ordos and Baikal clearly show the oldest initiation ages.

The period of tectonic quiescence, that time between the last major period of tectonism and initiation of the current extensional regime, is displayed in **Figures 14a**. **Figures 14b and c** show the same information as a function of individual basin sizes for the extensional regimes in continents and oceans, respectively. Basins in the respective regions are approximated as sharing the same period of quiescence There appears a tendency for the largest continental basins to be greater in those regions characterized by the longest periods of preceding crustal stability and the smallest where the preceding period of quiescence is least. The progression though is irregular and certainly not perfect. The ocean basins, again in stark contrast, offer an inverse relationship between basin size and the years of preceding crustal stability. The extensional basins of the Mid-Atlantic are among the largest of those studied and imprinted on rocks less than ~1 m.y., while much smaller basins along the Japan trench are imprinted seafloor previously undisturbed for ~140 ma.

The ages of most *Recent Volcanism* are not so amenable to presentation with this format of plots because they fail to characterize the extent of volcanism. Thus for example, recent volcanism is apparent along portions of the African Rift and absent in large portions as well, without an obvious difference in the first order manifestations of basins forming the Rift. Similarly, some minor young volcanics are found near one basin of the Ordos, but not in others. Plots of the age of recent volcanism and recent Volcanism versus basin area are nonetheless plotted for sake of completeness in **Figures 15a and b**, respectively.

Cumulative Extension and Strain

It is assumed here for purposes of comparison that normal faults bounding basins are planar and dip at angle θ between 50°-70°, and that measured values of structural relief are equivalent to vertical separations VS across the respective basin bounding faults. In this manner, extension E across a basin bounding fault is equal to $VS/\mathrm{Tan}(\theta)$. Estimates of extension made in this manner are problematic. Dips and geometries of bounding faults are generally not well known as they extend through the crust. It has long been discussed hat

some may be planar whereas others might be listric (e.g.,Stewart, 1971; 1978). Likewise, the orientations of basin bounding faults have been considered to rotate with continued displacement (e.g., Jackson and McKenzie, 1983). Isostatic forces have as well been cited to augment observed uplifts and rotate mountains and their bounding faults with the accumulation of slip over time (e.g., Ebinger et al., 1999). Granted the potential complexity of the process, the instrumental record of moderate and large normal earthquake ruptures shows rupture planes almost invariably approximated as planar and of moderate to steep dip within the crust (White et al., 1986; Doser and Smith, 1989; Jackson and White, 1989). Complimentary to that, one may allude to Anderson's early analyses (Anderson, 1905; 1951) based on frictional considerations and principles of Mohr-Coulomb theory that the optimal dip normal faults should be near 60°. That all said and given that the physics of normal faulting is shared between regions, the approach provides a manner to systematically compare relative, if not absolute, values of extension across basins of each region.

Calculated values of extension across all basins are displayed versus plot number in **Figure 16a**. Values of extension, be it the maximum or medial values for the continental regions, tend to increase in concert with the average size of basins registered in the respective regions. It is to be expected that increasing amounts of extension result in larger basins. The relationship of individual basin sizes to the extension registered in the respective basin is tendered in **Figures 16b and c** for the continental and marine basins, respectively. The distribution of continental basin sizes may be fit as a power law distribution, as can the data from individual regions within both the continental (**Figure 16b**) and oceanic (**Figure 16c)** environments. The data taken together show basin sizes to consistently increase with extension, though patterns of increase distinctly different between the separate regions.

Summing individual basin extensions along transects leads to the estimates of cumulative extension across the regions shown in **Figure 17a**. The basins defining the transects are given in the tables for each region and the distance along the transects plotted in **17b**. (Cumulative extension is taken to be equal to the individual basin extension in those instances where regional extension across a region is accommodated by only a single basin). Error bars reflect estimates assuming 50° and 70° dips. Drawing immediate attention is the significantly greater extension accommodated across the Basin and Range, with median estimate of the order of ~140 - 180 km. Median values of total extension in other regions reach no more than ~60 km. Dividing the measures of extension by transect length gives a measure of accumulated strain (or percent extension) and is plotted in **Figure 17c.** Maximum values of strain range between <0.1 to ~0.4 across the continental regions. There is a suggestion that areas of greater average basin size correspond to those areas exhibiting the greatest strains, but the low values of strain calculated across the East African Rift offer a clear exception to the trend. As well, given the added and unaccounted for uncertainty associated with defining the transect lengths, it is problematic to assess any possible systematics with confidence. Finally, it is notable that the largest values of cumulative strain appear along the Mid-Atlantic Ridge.

It is not intuitive how or if ongoing rates of extension or extensional strain should impact the physical expression of basins in a region. Geodetic extension and strain rates are nevertheless presented in **Figures 18a and 18b,** respectively, to assuage any questions that might arise concerning their impact on basin development. The highest rates of extension are being recorded being recorded across Tibet and across the Mid-Atlantic Ridge, reaching values in excess of 20 mm/yr. More common are rates <5 - 6 mm/yr. Contemporary strain rates vary by orders of magnitude across the various extensional provinces, with values in excess of 1000 nanostrain/yr across the Mid-Atlantic to less than 10 nanostrain/yr across the Basin and Range Province.

Tectonics

Descriptions sufficient for first order comparisons between the mechanisms of crustal deformation in each of the extensional regions constitute the body of this section. Sources, discussion, and additional illustrations on which the descriptions are based are detailed in the Appendix.

Faulting, basin development, and regional tectonics are commonly described within the framework of crustal stresses acting in the regions. Crustal stresses have long been depicted as orthogonally oriented maximum, minimum, and intermediate stress axes, commonly denoted as σ_{max}, σ_{min}, and σ_{int}, respectively. Within the crust one of these axes is generally oriented vertically and attributable only to gravity (e.g., Anderson, 1905; 1951). Normal faults and crustal extension are limited to regions where σ_{max} is the vertically oriented gravitational stress (**Figure 19**). Varying between the regions are the manner of crustal movements and deformation leading to this trait.

The Apennines of Italy are considered the result of crustal thickening accompanying subduction of the Adriatic Plate beneath the Tyrrhenian Sea since the Miocene (Malinverno and Ryan, 1986; Carminati et al., 2010) (**Figure 20**). The process of subduction has continually slowed since the Miocene (e.g., Handy et al., 2010; D'Agostino, 2014; Le Breton et al., 2017). The slowing has presumably been accompanied by reductions in contractional stress imposed by subduction relative to the gravitational stress developed with uplift of the Apennines. Within the high elevations of the Apennines the vertically oriented gravitational stress is now greater than horizontal tectonic stresses imposed by subduction (D'Agostino et al., 2014). The affinity of active normal faults and seismicity to the higher elevations of the Apennines that is observed today points to gravity as the primary factor producing extension in the Apennines (D'Agostino et al., 2014). Processes of trench roll back and back-arc spreading have also been suggested as mechanisms serving to reduce horizontal compressive stresses across the Apennines (Malinverno and Ryan, 1986).

Active extensional basins in Tibet occur in crust elevated and overthickened as the result of convergence of India beneath Eurasia (**Figure 21**) (Molnar and Tapponnier, 1977). Gravity and seismic data suggest isostatic forces are now balancing and limiting further uplift of the region (Lyon-Caen and Molnar, 1985; Molnar and Lyon-Caen, 1988; England and Houseman, 1989). The high elevations of the region are sufficient to yield gravitational stresses within the upper crust that are greater than horizontal contractional stresses resulting from the ongoing convergence of India into Eurasia (e.g., Molnar and Tapponnier, 1978; England and Houseman, 1989; Liu and Yang, 2003). In this regard, gravity is the principal stress driving the extension observed in Tibet today,

The genesis of extension in Basin and Range province **(Figures 1 and 2d)** shares aspects similar though distinct from that attributed to the extensional areas of Italy and Tibet. The region was characterized by an eastward subduction of the Pacific Plate beneath the North American Plate of the western United States leading up to the Miocene (Atwater, 1970; Atwater and Stock, 1998) (**Figure 22**). The convergence, as in the Apennines and Tibet, resulted in thickening and elevating the crust that now comprises the Basin and Range (Coney, 1987; Wolfe and Molnar, 1997; Garside et al., 2005; Henry et al., 2012). Miocene plate motions then resulted in the convergent boundary transforming to strike-slip along the San Andreas fault system and, in this manner, is considered to have reduced or removed the contractional stresses previously attendant to subduction (Dickenson and Snyder, 1979; Severinghaus and Atwater, 1990). Extension today is, like in the Apennines and Tibet, considered to be driven by the increased gravitational stress imparted by the relatively high regional elevation but also distributed shear related to the San Andreas (Jones et al., 1996; Sonder and Jones, 1999; Thatcher et al., 1999). The northwest directed shear adds a northwest oriented component of extension across the province that would not arise from gravity alone.

Extension in Aegean is also attributed to multiple factors though, in contrast to the preceding areas, neither are related to increases in vertical stress due to rises in elevation. Northerly extension is surmised to have initially been driven by a southward migration and development of a back arc basin behind the Hellenic Arc

that commenced sometime subsequent to ~35 Ma (Le Pichon and Angelier, 1979; Jolivet et al., 2013) (**Figure 23)**. A westward movement of Anatolia subsequently commenced along the right-lateral Anatolian fault system ~12 Ma (Sengor et al., 2005). The strike-slip motion of the Anatolian system is partitioned to additional extensional displacement within the Aegean along the westward reaches of the fault system (e.g., Armijo et al., 1999; Goldsworthy et al., 2002). In this instance then, it is horizontal crustal movements reducing horizontal stresses relative to those produced by gravity that result in the observed extension, not relatively increased gravitational stresses imparted by a relative increase in elevation.

Extension in Baikal and the Ordos share similar tectonic settings (**Figure 24**). Each is located at the end of major left-lateral strike systems that are in part accommodating crustal deformation resulting from collision of India into Eurasia. In these instances, the extensional Baikal and Ordos fault systems are accommodating lateral displacements at the ends of the respective strike-slip systems (Tapponnier and Molnar, 1977; Tapponnier and Molnar, 1979). The extensions are thus not driven by absolute increases in gravitational stress but rather the relative reduction of horizontal stresses produced by ongoing strike-slip motions.

The East African Rift System is generally discussed in a plate tectonic framework and considered a continuation of mid-ocean ridges and thus the result of incipient seafloor spreading (Girdler et al., 1969; McKenzie et al., 1970) (**Figures 1 and 25**). The primary forces driving extension are usually surmised to be plate tectonic motions and mantle flow associated with those motions, and not gravitational. The occurrence of mountains along the rift system is usually attributed to isostatic rebound linked to the reduction in vertical load resulting from fault displacement on the rift-bounding faults (Weissel and Karner, 1989; Ebinger et al., 1991). The increase in gravity accompanying the relative uplift may contribute to the extension, though the location of the East African Rift System within a circumference of seafloor spreading ridges (**Figure 1**) seems to require that horizontal tectonic displacements, not gravity, are the primary contributors to the observed extension. *Extension along the Mid-Atlantic Ridge* is attributed to the same processes as those along the East African Rift, though differentiated by occurring in much thinner crust and the presence of active volcanism **(Figure 26).**

The processes leading to *extension along the Japan Trench* are unique among the extensional environments. Graben development is limited to that area of the subducting plate exhibiting maximum curvature **(Figure 27)**. The bending stresses in the upper portion of the plate as it enters the trench are generally cited as responsible for horizontal stresses within the plate being less than those imposed by gravity (Jones et al., 1978; Chapple and Forsyth, 1979; Forsyth, 1982).

Insights, Inferences and Interpretations

The areal extent of active normal fault-bounded basins varies markedly between extensional provinces (**Figure 5**). The differences reach orders of magnitude, commonly with no overlap between those regions exhibiting the largest and smallest basins. It is natural to consider that physical characteristics of the crust play a causal role leading to the differences. It is true for example on the continents that the areal extent of basins tends to increase in concert with measured depths of Mojo and, hence, thickness of the crust (**Figures 10**). Exceptions to this trend are though conspicuous. The basins of Tibet are for example among the smallest of all regions considered but located where crustal thickness is twice that in the other regions. Echoing that point, basins in the two marine environments share similarly thin crust (**Figure 10ab**) but extremely different ranges of basin size (**Figure 5**). Similar inconsistencies arise when considering regional heat flow (**Figure 11**), the time when extension commenced (**Figure 13**), the age of any major preceding tectonic events (**Figure 14**), and the age and extent of volcanism (**Figure 15**) in relation to the range of basin sizes in the respective areas. From this it is inferred that, while contributing, none of these factors can be the principle control leading to the marked difference in areal extent of basins observed between the extensional provinces.

In some contrast, when taking the observations of all continental regions together and those in the oceans separately, measures of aspect ratio (**Figures 6a and 7abcd**), structural relief (**Figure 8bcd**), and estimated values of extension (**Figure 16ab**) in individual basins appear to progressively increase in concert with the spatial dimensions of basins. Because estimates of extension are geometrically derived from measures of structural relief, it is to be expected they show similar progressive increases with respect to basin area. Also observed and plotted in **Figure 9abc** is a similar tendency for structural relief to increase with basin length across the aggregate of all basins, but for the Japan Trench where the tendency is not evident. The increase in structural relief with basin length may be expected in light of numerous studies that have shown a relationship between fault displacement and fault length (e.g., Scholz and Cowie, 1990; Scholz et al., 1993; Lathrop et al., 2022).

Regression lines in the form of power laws serve to illustrate the positive relationship between basin area and aspect ratio (**Figure 7**), structural relief (**Figure 8**), and extension (**Figure 16**), and that the relationships differ between the continental and oceanic extensional areas. Similar is done for the relationship between structural relief and basin length in **Figure 9**. It is logical to suggest that the regressions reflect a singular physical mechanism whereby (1) basin areas grow systematically as a function of accumulating displacement and extension and (2) that the growth occurs preferentially in the length direction (i.e. aspect ratios increase). Some observations though suggest caution be applied to such an interpretation. For example, increases in aspect ratio with basin area are not observed when considering separately the the regions of continental extension (**Figures 7e-j**). As well, the regression lines in **Figures 8, 9**, and **16** are fit through fields of points derived from the various extensional regions for which basin areas often show little to no overlap, and regressions through separate regions yield varying scaling exponents. In sum, while pointing toward systematics in the growth of basins, the regressions do not by themselves provide an answer to why, as observed in **Figure 5**, there exist such large differences in basin dimensions between the various extensional provinces. Other mechanisms must be contributing. That said, one may also rule out the estimates of cumulative extension and strain across the regions (**Figure 17**). Neither exhibit a regular increase with the average size of basins.

Review shows extension in Italy **(Figure 20)** and Tibet **(Figure 21)** is driven primarily by increased gravitational stress resulting from convergent tectonic processes that have led to regional increases in elevation. In an opposite sense, extension along the Japan Trench is attributed to bending of the seafloor as it subducts beneath Japan, yielding stresses at the points of maximum bending sufficient to reduce horizontal compressive stresses in the crust to less than those imposed vertically by gravity **(Figure 28)**. Extension in Africa **(Figure 27)**, Baikal and the Ordos **(Figure 24)**, and the Mid-Atlantic Ridge **(Figure 26)** are in contrast driven primarily by singular and horizontally directed tectonic motions. Finally, extension in the Basin and Range and the Aegean is driven by a combination or hybrid of gravity and horizontally directed crustal motions.

Each of the regions is graphically shown as a function of the median basin size observed for each region as shown in **Figure 5.** The extensional regions with the largest basins (Africa, Baikal, and the Ordos) are thus those resulting primarily from horizontally directed crustal motions. Extension in those regions displaying the smallest basins is driven by gravity (Tibet and Italy) or the localized reduction in horizontal stresses (Japan Trench), and extension in those regions displaying an intermediate range of basin sizes (Basin and Range and the Aegean) is driven by a hybrid of the preceding mechanisms.

In this context, the small basins of Italy, Tibet, and the Japan Trench may be attributed to self limiting processes that have led to gravity being the maximum principal stress. Normal faulting in Italy and Tibet for example serves to thin and lessen elevation of the crust and thus reduce the very energy needed for continued basin growth. The process is exacerbated in Italy by the ongoing reduction in the rate of Adriatic plate subduction and in the Himalaya because isostatic forces appear to be limiting future uplift of Tibet. Similarly

along the Japan Trench, the amount of extension is limited by the relatively short time any portion of the subducting plate is situated in the region of maximum curvature. Conversely, in the regions Africa, Baikal, and the Ordos which display the largest basins, there is no obvious limit to the horizontally directed crustal motions driving the extension and greater basin growth is allowed and expected. It thus seems at the end of this comparative view that it is the tectonic framework, rather than geophysical characteristics of the crust or rates and amounts of extension, that is the primary factor responsible for the differing ranges of basin sizes exhibited between the globe's major regions of crustal extension..

Acknowledgments

Thanks are in order to Daniela Pantosti, Alessandro Michetti, Peizhen Zhang, Olaf Zielke, and Martin Mai. With them in Italy, China and Africa while on sabbatical leave, I was introduced first-hand vast disparity in basins sizes that exist between regions of active normal faulting. Christie Rowe graciously allowed time and space to pursue the project, and Graham Kent made sure to make me finish.

References Cited

Amante, C., and W. Eakins, (2009). ETOPO1 1 Arc-Minute Global Relief Model: Procedures, Data Sources and Analysis. NOAA Technical Memorandum NESDIS NGDC-24 National Geophysical Data Center, NOAA.

Anderson, E. M., (1905). The Dynamics of Faulting. Transactions of the Edinburgh Geological Society. 8, 387-402.

Anderson, E. M., (1951). The Dynamics of Faulting and Dyke Formation with Applications to Britain, Oliver and Boyd, Edinburgh, pp.

Armijo, R., B. Meyer, A. Hubert, and A. Barka, (1999). Westward propagation of the North Anatolian fault into the northern Aegean: Timing and kinematics. Geology. 27, 3, 10.1130/0091-7613(1999)027<0267:wpotna>2.3.co;2, 267-270.

Atwater, T., (1970). Implications of plate tectonics for the Cenozoic tectonic evolution of western North America. Bulletin of the Geological Society of America. 81, 3513-3536.

Atwater, T., and J. Stock, (1998). Pacific North America plate tectonics of the Neogene southwestern United States: An update. International Geology Review. 40, 5, 375-402.

Carminati , E., M. Lustrino, M. Cuffaro, and C. Doglioni (2010). Tectonics, magmatism and geodynamics of Italy: What we know and what we imagine, in *The Geology of Italy: tectonics and life along plate margins* M. Beltrando, A. Peccerillo, M. Mattei, S. Conticelli and C. Doglioni (Editors), Journal of Virtual Explorer, Electronic Edition, paper 9.

Cavinato, G. P., and P. G. De Celles, (1999). Extensional basins in the tectonically bimodal central Apennines fold-thrust belt, Italy: Response to corner flow above a subducting slab in retrograde motion. Geology. 27, 10, 10.1130/0091-7613(1999)027<0955:ebittb>2.3.co;2, 955-958.

Cemen, I., (2010). Extensional tectonics in the Basin and Range the Aegean, and Western Anatolia: Introduction. Tectonophysics. 488, 1-4, 10.1016/j.tecto.2010.05.002, 1-6.

Chapple, W. M., and D. W. Forsyth, (1979). Earthquakes and bending of plates at trenches. Journal of Geophysical Research. 84, NB12, 10.1029/JB084iB12p06729, 6729-6749.

Chiarabba, C., J. L., and R. DiStefano, (2005). A new view of Italian seismicity using 20 years of instrumental recordings. Tectonophysics. 395, 251-268.

Chiaraluce, L., C. Chiarabba, C. Collettini, D. Piccinini, and M. Cocco, (2007). Architecture and mechanics of an active low-angle normal fault: Alto Tiberina Fault, northern Apennines, Italy. Journal of Geophysical Research-Solid Earth. 112, B10, 10.1029/2007jb005015, 22.

Coney, P. J. (1987). The regional tectonic setting and possible causes of Cenozoic extension in the North American Cordillera, in *Continental extensional tectonics* M. P. Coward, J. F. Dewey and P. L. Hancock (Editors), Geological Society of London,, London, 177-186.

D'Agostino, N., (2014). Complete seismic release of tectonic strain and earthquake recurrence in the Apennines (Italy). Geophysical Research Letters. 41, 4, 10.1002/2014gl059230, 1155-1162.

D'Agostino, N., P. England, I. Hunstad, and G. Selvaggi, (2014). Gravitational potential energy and active deformation in the Apennines. Earth and Planetary Science Letters. 397, 10.1016/j.epsl.2014.04.013, 121-132.

Dawers, N. H., M. H. Anders, and C. H. Scholz, (1993). Growth of normal faults - displacement-length scaling. Geology. 21, 12, 10.1130/0091-7613(1993)021<1107:GONFDL>2.3.CO;2, 1107-1110.

Dickenson, W. R., and W. S. Snyder, (1979). Geometry of subducted slabs related to San Andreas transform. Journal of Geology. 87, 609-628.

Doser, D. I., and R. B. Smith, (1989). An assessment of source parameters of earthquakes in the Cordillera of the Western United-States. Bulletin of the Seismological Society of America. 79, 5, 1383-1409.

Ebinger, C. J., J. A. Jackson, A. N. Foster, and N. J. Hayward, (1999). Extensional basin geometry and the elastic lithosphere. Philosophical Transactions of the Royal Society a-Mathematical Physical and Engineering Sciences. 357, 1753, 741-762.

Ebinger, C. J., G. D. Karner, and J. K. Weissel, (1991). Mechanical strength of extended continental lithosphere - constraints from the Western Rift System, East-Africa. Tectonics. 10, 6, 10.1029/91tc00579, 1239-1256.

England, P., and G. Houseman, (1989). Extension during continental convergence, with application to the Tibetan Plateau. Journal of Geophysical Research. 94, B12, 10.1029/JB094iB12p17561, 17561-17579.

Forsyth, D. W., (1982). Determinations of focal depths of earthquakes associated with the bending of oceanic plates at trenches. Physics Of The Earth And Planetary Interiors. 28, 2, 10.1016/0031-9201(82)90079-6, 141-160.

Garside, L. J., C. D. Henry, J. E. Faulds, and N. H. Hinz (2005). The upper reaches of the Sierra Nevada auriferous gold channels, California and Nevada, in *Geological Society of Nevada Symposium 2005: Window to the World* H. N. Rhoden, R. C. Steininger and P. G. Vikre (Editors), Geological Society of Nevada, Reno, Nevada, 1-27.

GEBCO, (2024). Compilation Group - General Bathymetric Chart of the Oceans (Global Terrain Model). Grid (doi:10.5285/1c44ce99-0a0d-5f4f-e063-7086abc0ea0f). http://www.gebco.net.

Girdler, R. W., J. D. Fairhead, R. C. Searle, and Sowerbut.Wt, (1969). EVOLUTION OF RIFTING IN AFRICA. NATURE. 224, 5225, 10.1038/2241178a0, 1178-&.

Goldsworthy, M., J. Jackson, and J. Haines, (2002). The continuity of active fault systems in Greece. Geophysical Journal International. 148, 3, 10.1046/j.1365-246X.2002.01609.x, 596-618.

Handy, M. R., S. M. Schmid, R. Bousquet, E. Kissling, and D. Bernoulli, (2010). Reconciling plate-tectonic reconstructions of Alpine Tethys with the geological-geophysical record of spreading and subduction in the Alps. EARTH-SCIENCE REVIEWS. 102, 3-4, 10.1016/j.earscirev.2010.06.002, 121-158.

Henry, C. D., N. H. Hinz, J. E. Faulds, J. P. Colgan, D. A. John, E. R. Brooks, E. J. Cassel, L. J. Garside, D. A. Davis, and S. B. Castor, (2012). Eocene-Early Miocene paleotopography of the Sierra Nevada-Great Basin-Nevadaplano based on widespread ash-flow tuffs and paleovalleys. Geosphere. 8, 1, 10.1130/ges00727.1, 1-27.

Jackson, J., and D. McKenzie, (1983). The geometrical evolution of normal fault systems. Journal of Structural Geology. 5, 5, 10.1016/0191-8141(83)90053-6, 471-482.

Jackson, J. A., and N. J. White, (1989). Normal faulting in the upper continental crust: observations from regions of active extension. Journal of Structural Geology. 11, 1, 10.1016/0191-8141(89)90033-3, 15-36.

Jolivet, L., C. Faccenna, B. Huet, L. Labrousse, L. Le Pourhiet, O. Lacombe, E. Lecomte, E. Burov, Y. Denele, J.-P. Brun, M. Philippon, A. Paul, G. Salaue, H. Karabulut, C. Piromallo, P. Monie, F. Gueydan, A. I. Okay, R. Oberhaesli, A. Pourteau, R. Augier, L. Gadenne, and O. Driussi, (2013). Aegean tectonics: Strain localisation, slab tearing and trench retreat. Tectonophysics. 597, 10.1016/j.tecto.2012.06.011, 1-33.

Jones, C. H., J. R. Unruh, and L. J. Sonder, (1996). The role of gravitational potential energy in active deformation in the southwestern United States. Nature. 381, 6577, 10.1038/381037a0, 37-41.

Jones, G. M., T. W. C. Hilde, G. F. Sarman, and D. C. Agnew, (1978). Fault patterns in outer trench walls and their tectonic significance. Journal of Physics of the Earth. 26, Supplement, S85-S101.

Lathrop, B. A., C. A. L. Jackson, R. E. Bell, and A. Rotevatn, (2022). Displacement/Length Scaling Relationships for Normal Faults; a Review, Critique, and Revised Compilation. Frontiers in Earth Science. 10, 10.3389/feart.2022.907543, 907543.

501 Lavecchia, G., (2024). Slowly deforming megathrusts within the continental lithosphere: a case from Italy.
502 GSA Today. 34, 1-10.
503 Le Breton, E., M. R. Handy, G. Molli, and K. Ustaszewski, (2017). Post-20 Ma Motion of the Adriatic Plate:
504 New Constraints From Surrounding Orogens and Implications for Crust-Mantle Decoupling. Tectonics.
505 36, 12, 10.1002/2016TC004443, 3135-3154.
506 Le Pichon, X., and J. Angelier, (1979). The Hellenic arc and trench system: a key to the neotectonic evolution
507 of the eastern Mediterranean sea. Tectonophysics. 60, 1-42.
508 Liu, M., and Y. Q. Yang, (2003). Extensional collapse of the Tibetan Plateau: Results of three-dimensional
509 finite element modeling. Journal Of Geophysical Research. 108, B8, 10.1029/2002JB002248.
510 Logatchev, N. A., Y. A. Zorin, and V. A. Rogozhina, (1983). Baikal Rift - active or passive - comparison of
511 the Baikal and Kenya rift zones. Tectonophysics. 94, 1-4, 10.1016/0040-1951(83)90018-5, 223-240.
512 Lyon-Caen, H., and P. Molnar, (1985). Gravity-anomalies, flexure of the Indian Plate, and the structure,
513 support and evolution of the Himalaya and Ganga basin. Tectonics. 4, 6, 10.1029/TC004i006p00513,
514 513-538.
515 Malinverno, A., and W. B. F. Ryan, (1986). Extension in the Tyrrhenian sea and shortening in the Apennines
516 as result of arc migration driven by sinking of the lithosphere. Tectonics. 5, 2,
517 10.1029/TC005i002p00227, 227-245.
518 McKenzie, D. P., D. Davies, and P. Molnar, (1970). PLATE TECTONICS OF RED-SEA AND EAST-
519 AFRICA. NATURE. 226, 5242, 10.1038/226243a0, 243-&.
520 Molnar, P., and H. Lyon-Caen, (1988). Some simple physical aspects of the support, structure, and evolution
521 of mountain belts. Geological Society of America Special Paper. 218, 179-207.
522 Molnar, P., and P. Tapponnier, (1977). The collision between India and Eurasia. Scientific American. 236, 4,
523 30-41.
524 Molnar, P., and P. Tapponnier, (1978). Active tectonics of Tibet. Journal of Geophysical Research, A, Space
525 Physics. 83, B11, 5361-5375.
526 NOAA, (2022). ETOPO 2022 15 Arc-Second Global Relief Model. NOAA National Centers for
527 Environmental Information. 10.25921/fd45-gt74.
528 Pavlovsky, E. V., (1948). A comparison of the tectonics of Meso-Cenozoic structures of East Siberia and the
529 East African rift (in russian). Proc. Acad. Sci USSR. Ser. Geol, no. 5, 25-38.
530 Scholz, C. H., and P. A. Cowie, (1990). Determination of total strain from faulting using slip measurements.
531 Nature. 346, 6287, 10.1038/346837a0, 837-839.
532 Scholz, C. H., N. H. Dawers, J. Z. Yu, and M. H. Anders, (1993). Fault growth and fault scaling laws -
533 preliminary-results. Journal of Geophysical Research. 98, B12, 10.1029/93JB01008, 21951-21961.
534 Sengor, A. M. C., O. Tuysuz, C. Imren, M. Sakınç, H. Eyidogan, N. Görür, L. Pichon, and R. X., (2005). The
535 North Anatolian Fault: a new look. Annual Review of Earth and Planetary Sciences. 33, 37-112.
536 Severinghaus, J., and T. Atwater, (1990). Cenozoic geometry and thermal state of the subducting slabs
537 beneath western North America. Geological Society of America Memoir. 176, 1-22.
538 Sonder, L. J., and C. H. Jones, (1999). Western United States extension: How the West was widened. Annual
539 Review of Earth and Planetary Sciences. 27, 10.1146/annurev.earth.27.1.417, 417-+.
540 Stewart, J. H., (1971). Basin And Range Structure - System Of Horsts And Grabens Produced By Deep-
541 Seated Extension. Geological Society of America Bulletin. 82, 4, 10.1130/0016-
542 7606(1971)82[1019:barsas]2.0.co;2, 1019-1043.
543 Stewart, J. H. (1978). Basin and Range structure in western north America: A review, in *Cenozoic Tectonics and*
544 *Regional Geophysics of the Western Cordillera* R. B. Smith and G. P. Eaton (Editors), Geological Society of
545 America, Boulder, CO, 1-31.
546 Tapponnier, P., and P. Molnar, (1977). Active faulting and tectonics in China. Journal of Geophysical
547 Research. 82, 20, 10.1029/jb082i020p02905, 2905-2930.
548 Tapponnier, P., and P. Molnar, (1979). Active faulting and Cenozoic tectonics of the Tien Shan, Mongolia,
549 and Baykal regions. Journal of Geophysical Research. 84, NB7, 10.1029/JB084iB07p03425, 3425-&.
550 Thatcher, W., G. R. Foulger, J. B. R., J. Svarc, E. Quilty, and G. W. Bawden, (1999). Present-day deformation
551 across the Basin and Range province, western United States. Science. 283, 1714-1718.
552 Weissel, J. K., and G. D. Karner, (1989). Flexural uplift of rift flanks due to mechanical unloading of the
553 lithosphere during extension. Journal of Geophysical Research: Solid Earth. 94, B10,
554 10.1029/JB094iB10p13919, 13919-13950.

555 White, N. J., J. A. Jackson, and D. P. McKenzie, (1986). The relationship between the geometry of normal
556 faults and that of the sedimentary layers in their hanging walls. Journal of Structural Geology. 8, 8,
557 10.1016/0191-8141(86)90035-0, 897-909.
558 Wolfe, J. A., and P. Molnar, (1997). Paleobotannical evidence for high altitudes in Nevada during the Miocen.
559 Science. 276, 1672-1675.
560

Figures and Figure Captions

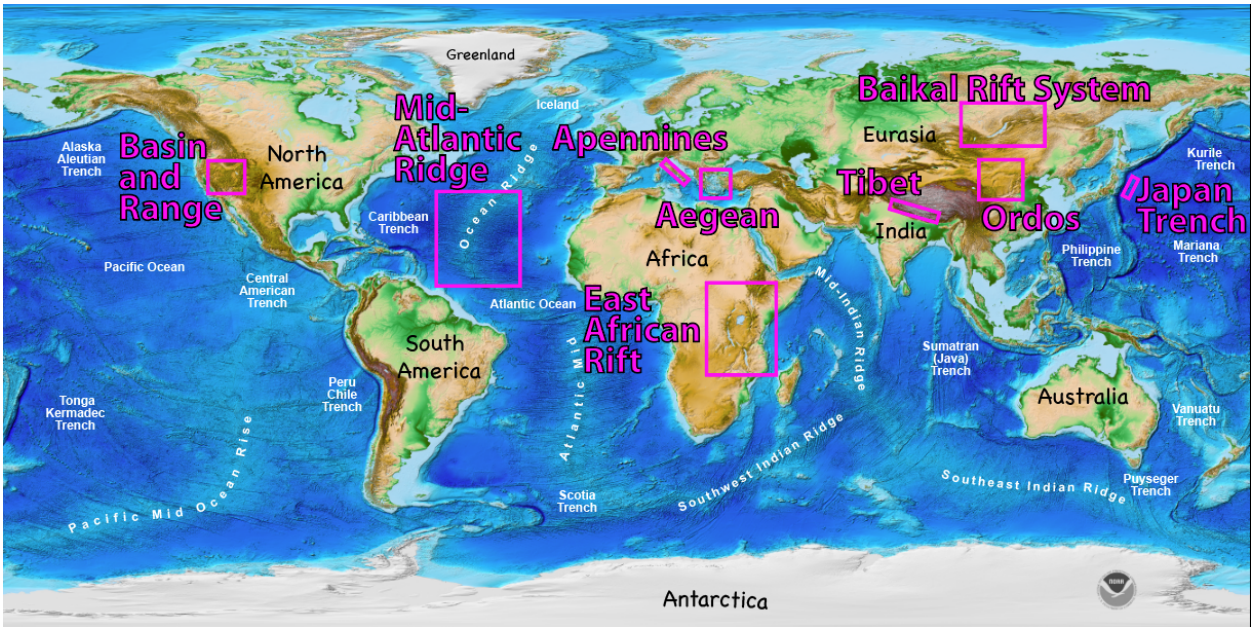

Figure 1. Areas characterized by active normal fault-bounded basins and crustal extension are labeled and delineated by magenta boxes. Adapted from Amante and Eakins (2009)and NOAA (2022)

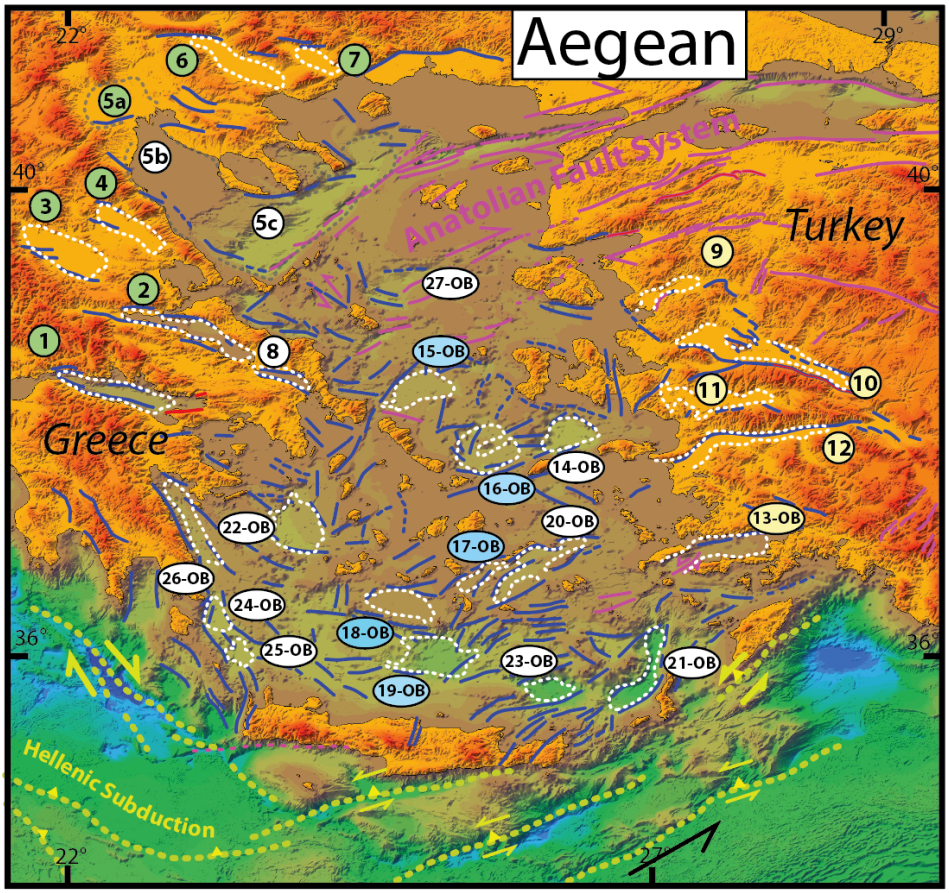

Figure 2a. Aegean Sea area. Normal and strike-slip fault lines blue and magenta, respectively. Faults of Hellenic Subduction Zone in yellow. Colored circles mark basins along transects discussed in text. Dashed white lines delineate area of basins. **(See text and full caption after Figure 2i)**

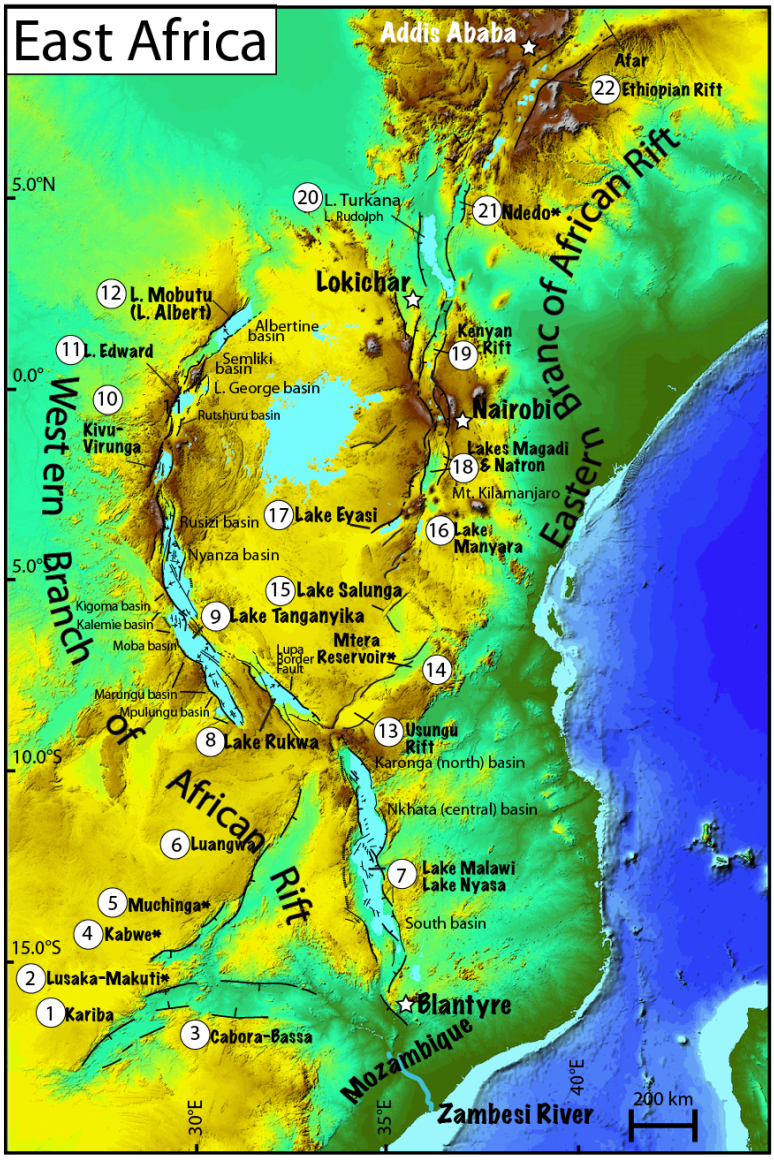

Figure 2b. East African Rift System. **(See text and full caption after Figure 2i)**

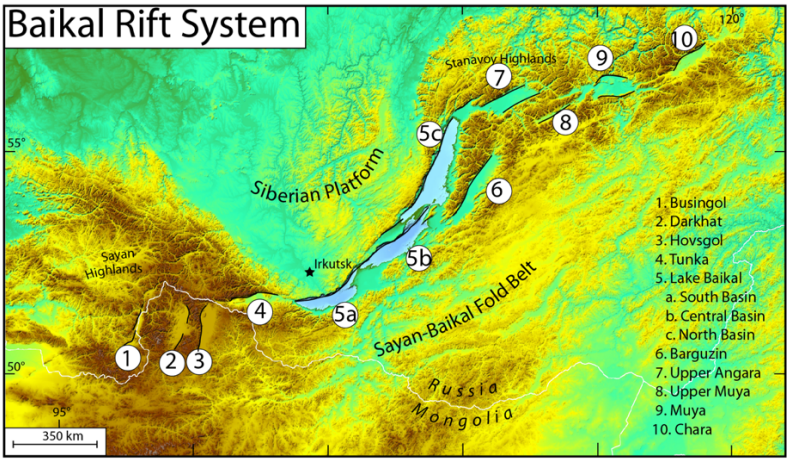

Figure 2c. Baikal Rift System **(See text and full caption after Figure 2i)**

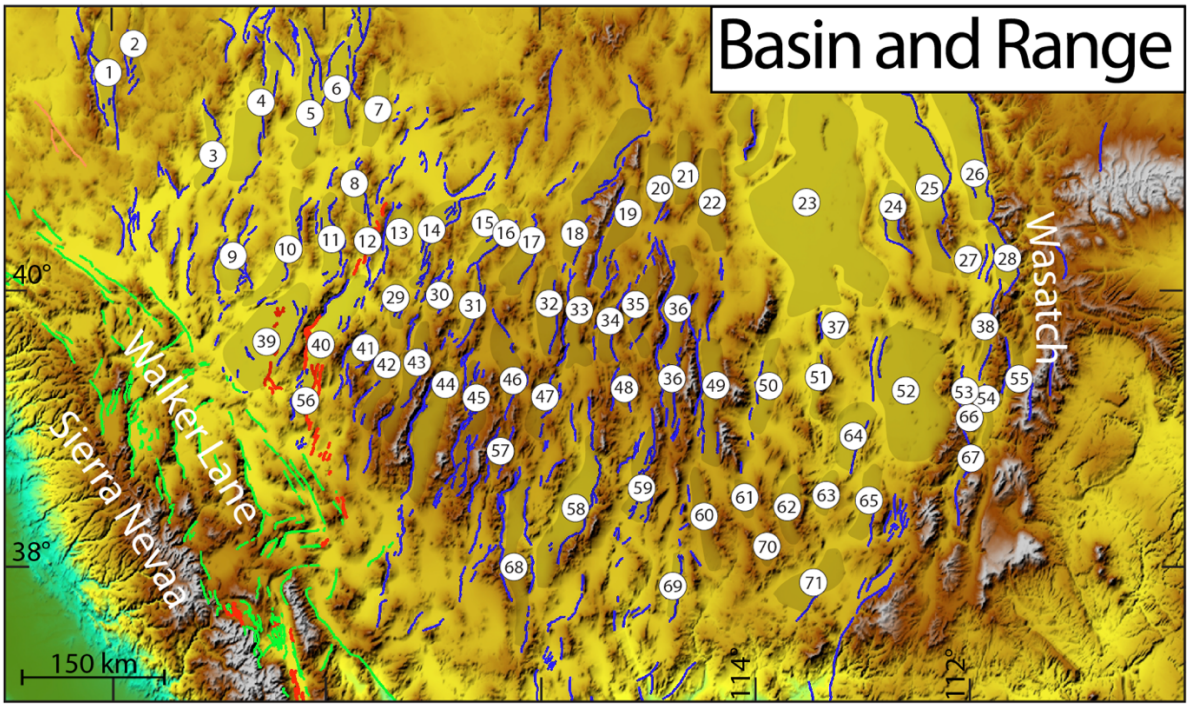

Figure 2d. Basin and Range. Normal and strike-slip fault lines blue and green, respectively. Historical surface ruptures in red. Areas of basins lightly shaded. **(See text and full caption after Figure 2i)**

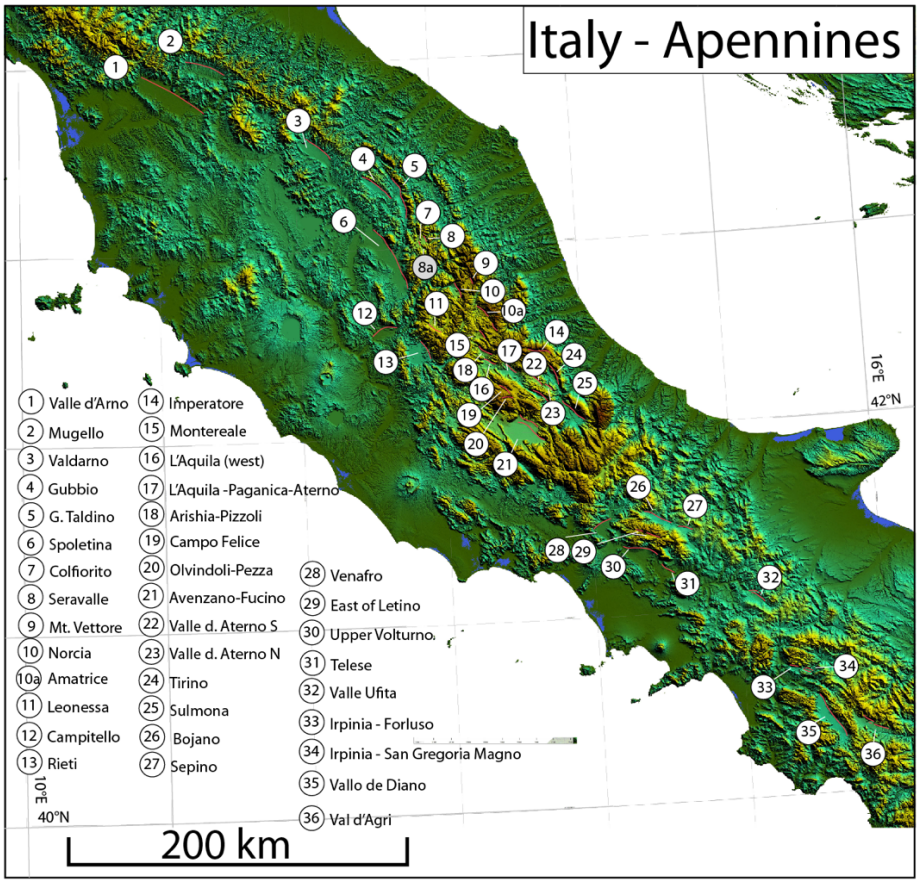

Figure 2e. Apennines of Italy. Active normal faults are thin red lines. **(See text and full caption after Figure 2i)**

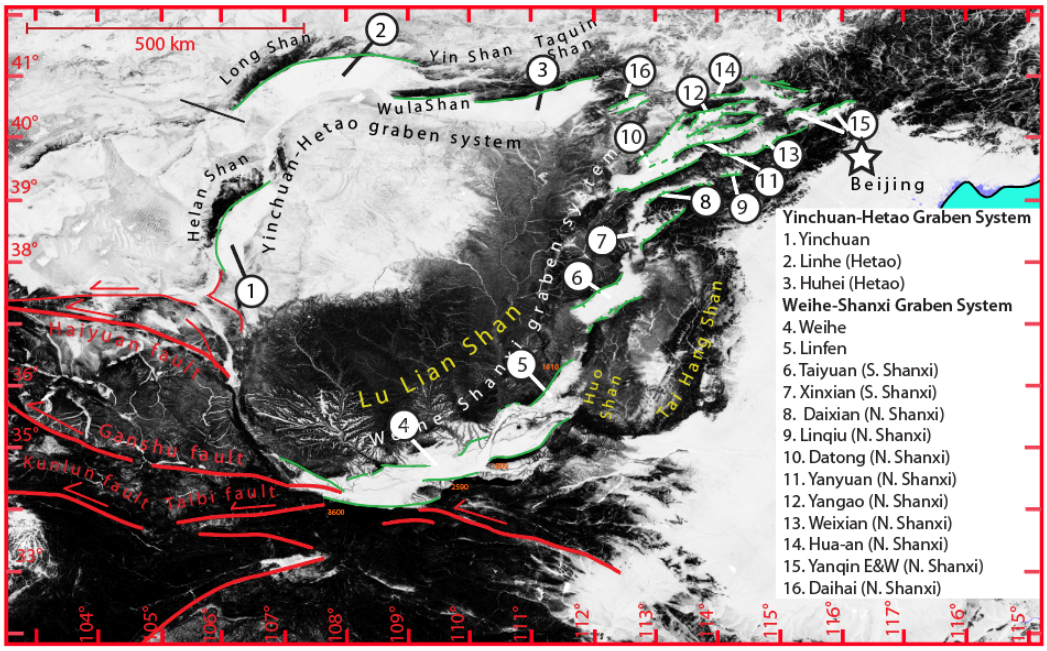

Figure 2f. Basins along perimeter of Ordos Plateau in China. **(See text and full caption after Figure 2i)**

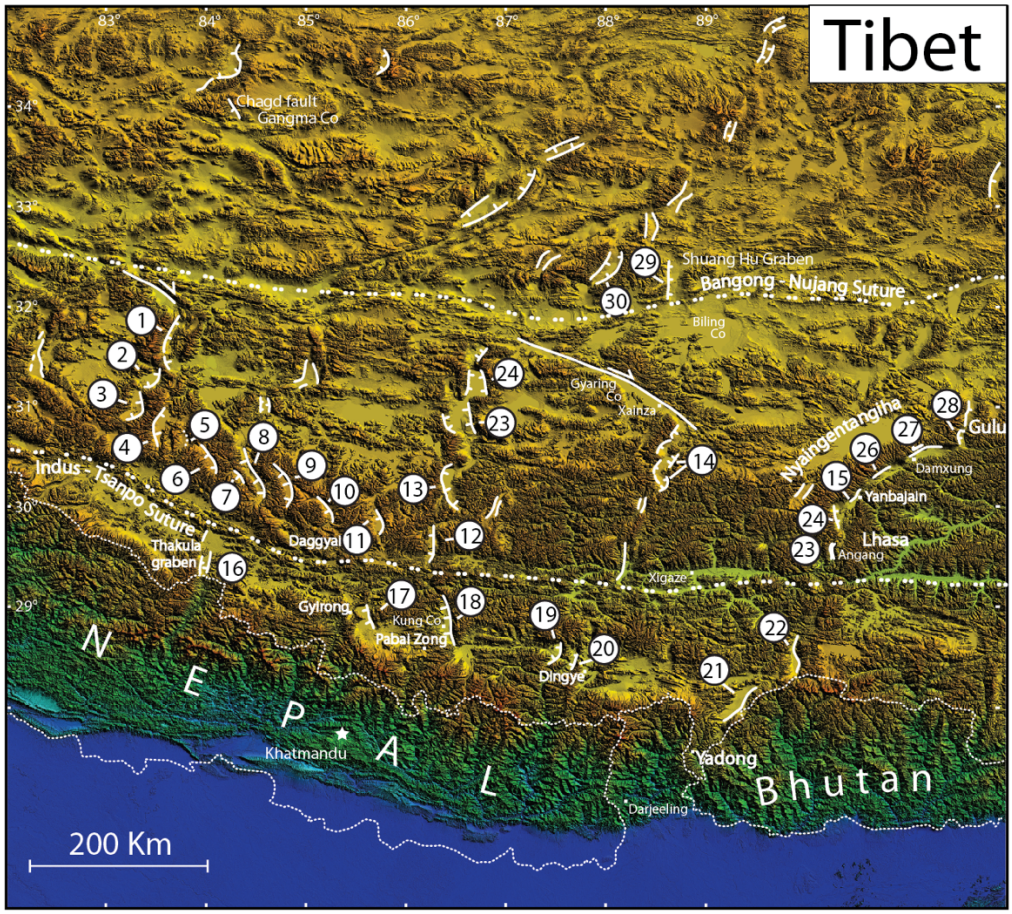

Figure 2g. Extensional basins of Tibet **(See text and full caption after Figure 2i).**

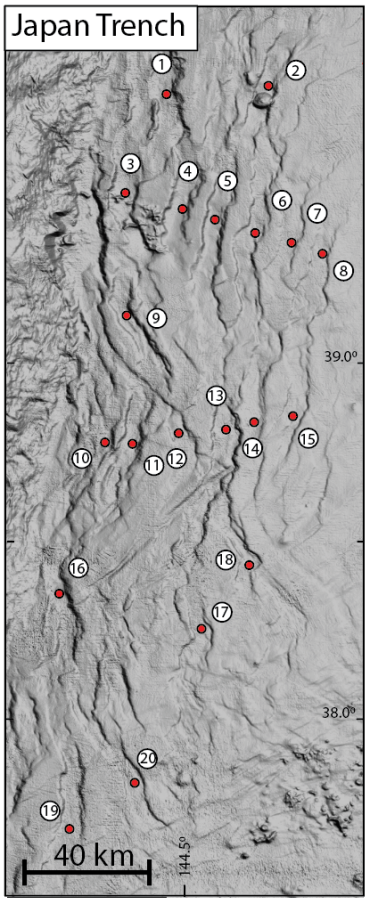

Figure 2h. Extensional basins along Japan Trench. Digital elevation model from GEBCO (2024) **(See text and full caption after Figure 2i).**

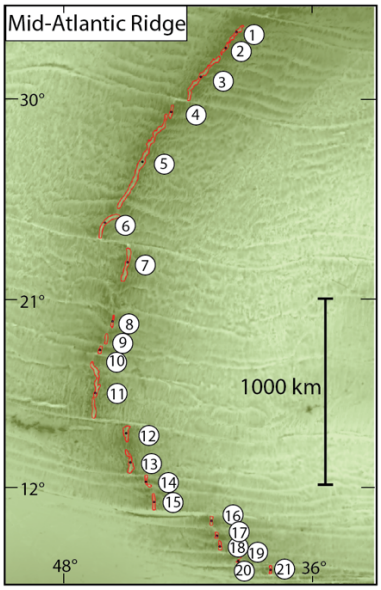

Figure 2i. Basins along Mid Atlantic Ridge. **(See text and full caption after Figure 2i)**

Figure 2 (Full Caption). Shaded relief and slope-shade maps of regions outlined in **Figure 1**. Alluvial and lake-filled basins bounded by active normal faults are generally manifest as smooth surfaces within the higher rugged relief of adjacent mountains. Basin numbers correspond to **Tables 1 through 9** wherein basin names and descriptive information for each are provided for the respective regions. Major faults bounding basins are marked by lines where known. **(a)** Aegean Sea area. Normal and strike-slip fault lines blue and magenta, respectively. Faults of Hellenic Subduction Zone in yellow. Colored circles mark basins along transects discussed in text. Dashed white lines delineate area of basins. **(b)** East African Rift system. **(c)** Baikal Rift system. **(d)** Basin and Range. Normal and strike-slip fault lines blue and green, respectively. Historical surface ruptures in red. Areas of basins lightly shaded. **(e)** Apennines of Italy. Active normal faults are red. **(f)** Basins along perimeter of Ordos Plateau in China. **(g)** Extensional basins of Tibet, **(h)** Japan Trench. Digital elevation model from GEBCO (2024) and **(i)** Mid-Atlantic Ridge.

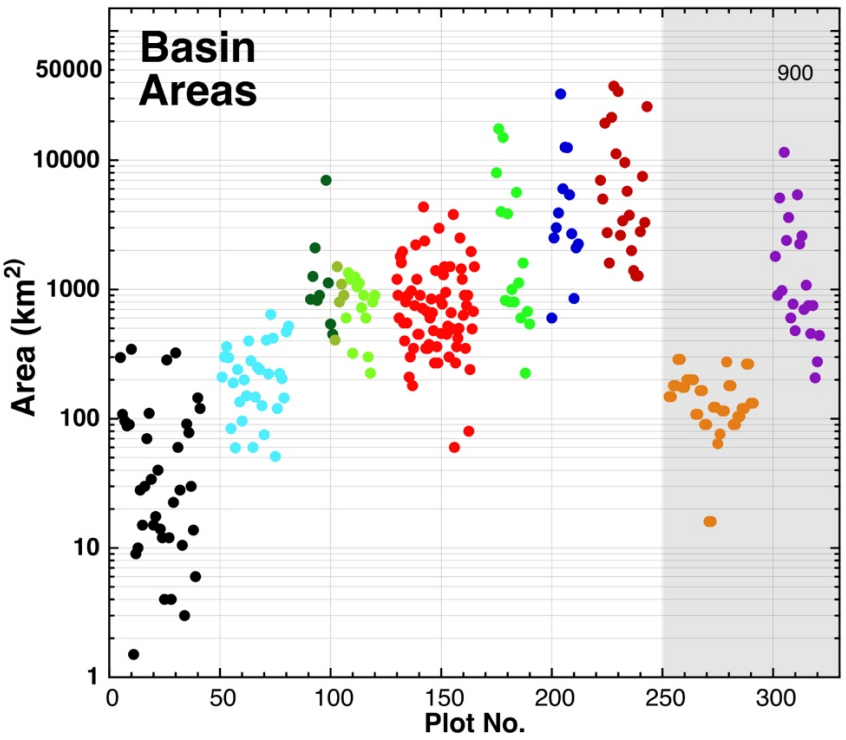

Figure 3. Manner of plotting observations. Map view areas of basins shown in **Figure 2** are plotted versus plot number. Basin values are color coded according to the region in **Figure 1** where the basin is located. Plot numbers are listed in **Tables 1 to 9** for the respective regions, wherein the plot number is linked to basin names and locations, and sources and methods of measurement of the plotted values are tabulated. Basins in continents are to left and those of two marine environments fall within the shading. Large differences within and between regions are evident and warrant explanation.

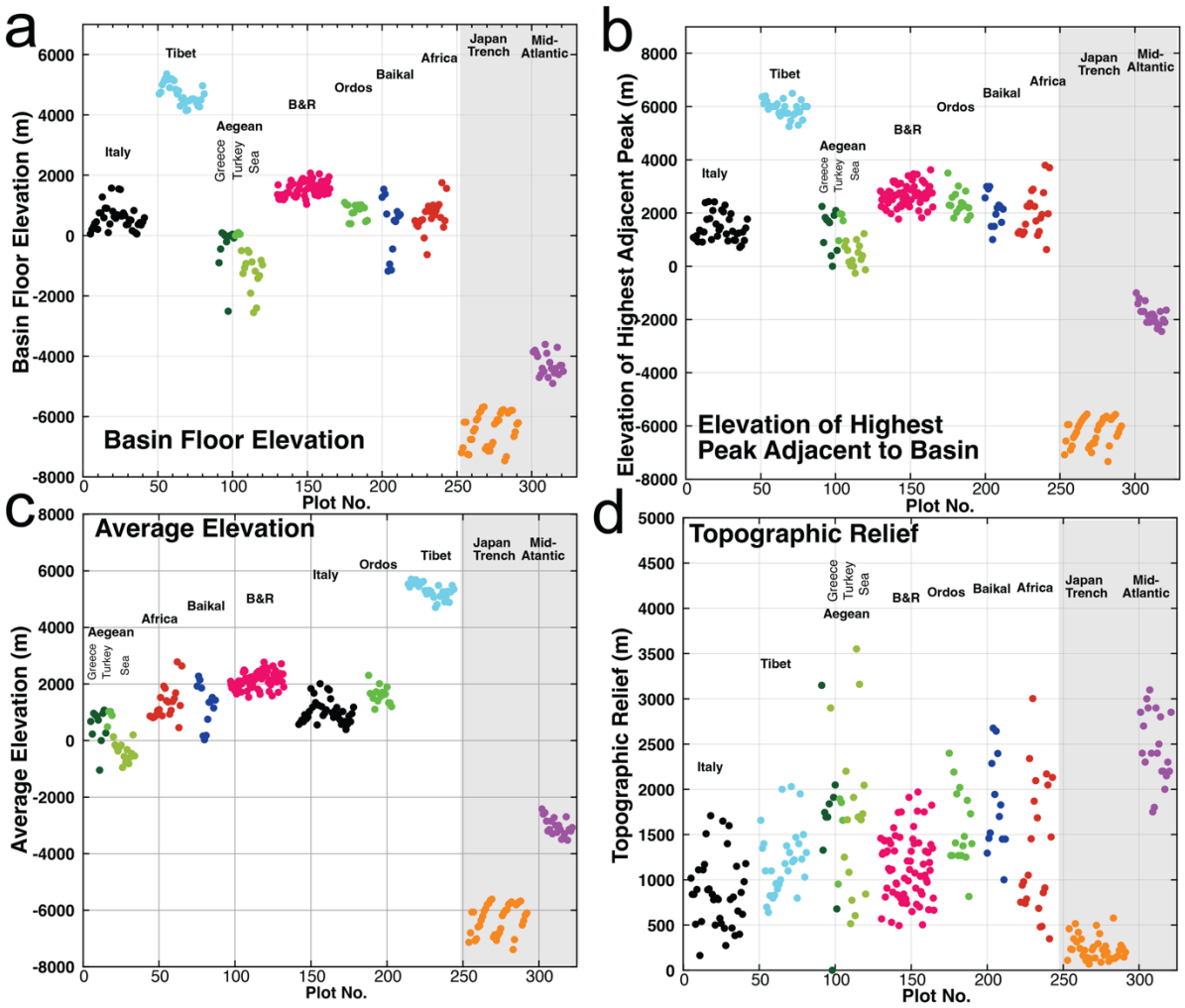

Figure 4. Elevations of (a) basin floor (b) adjacent highest peak, (c) averages of values in (a) and (b), and (d) topographic relief. Areas within oceanic crust shaded.

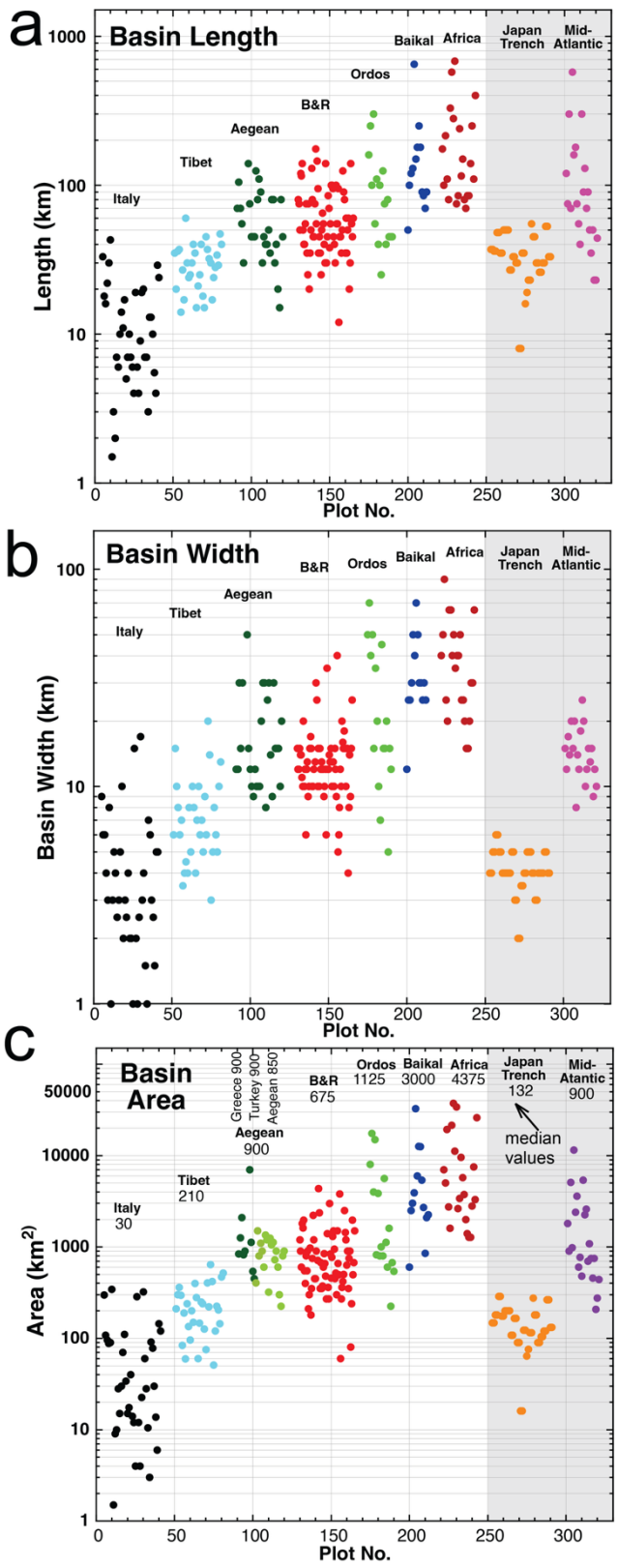

Figure 5. (a) Basin lengths, (b) basin widths, and (c) basin areas.

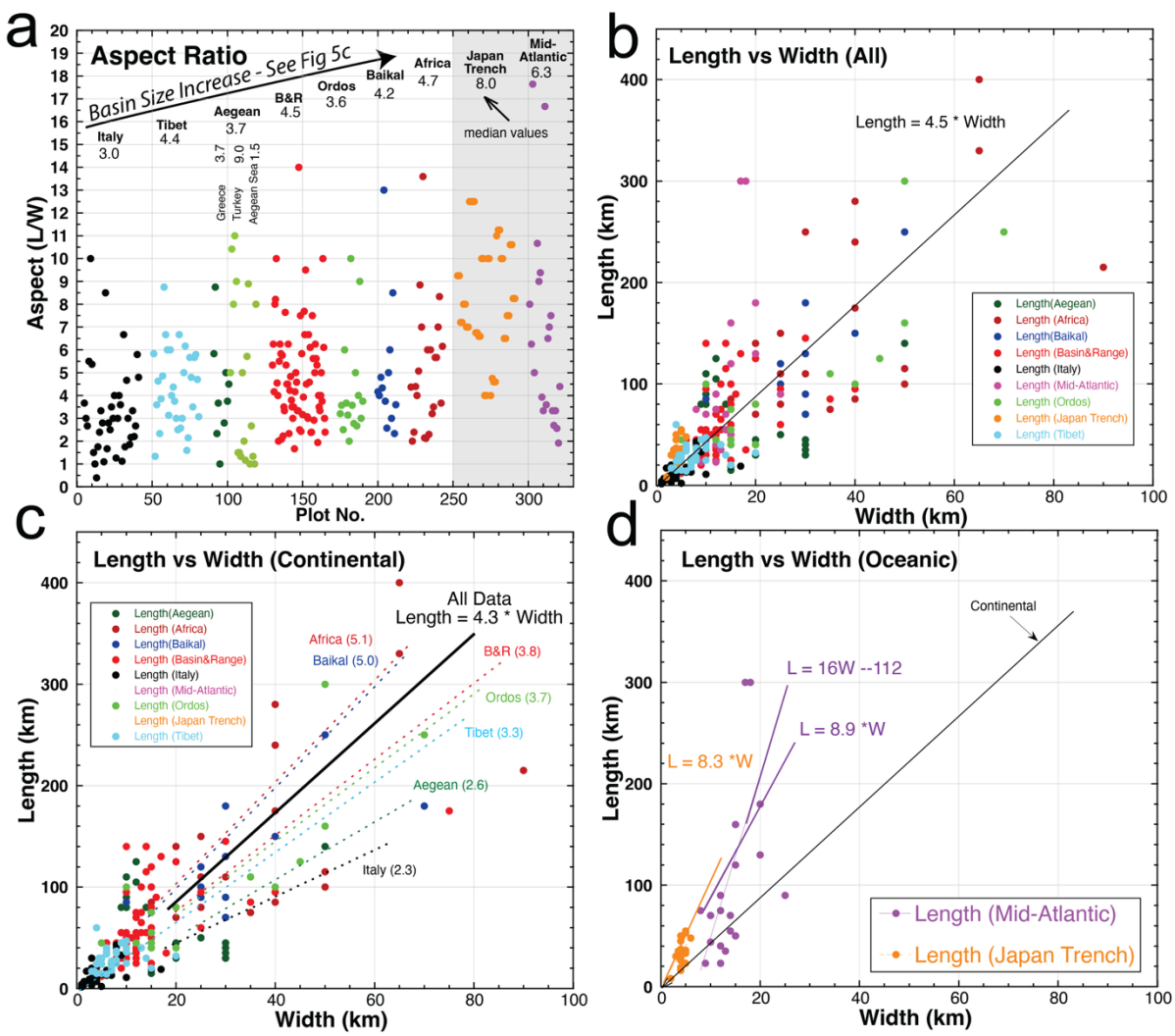

Figure 6. (a) Aspect ratio versus plot number. Basin lengths versus widths for (b) all basins, (c) continental basins, and (d) ocean basins.

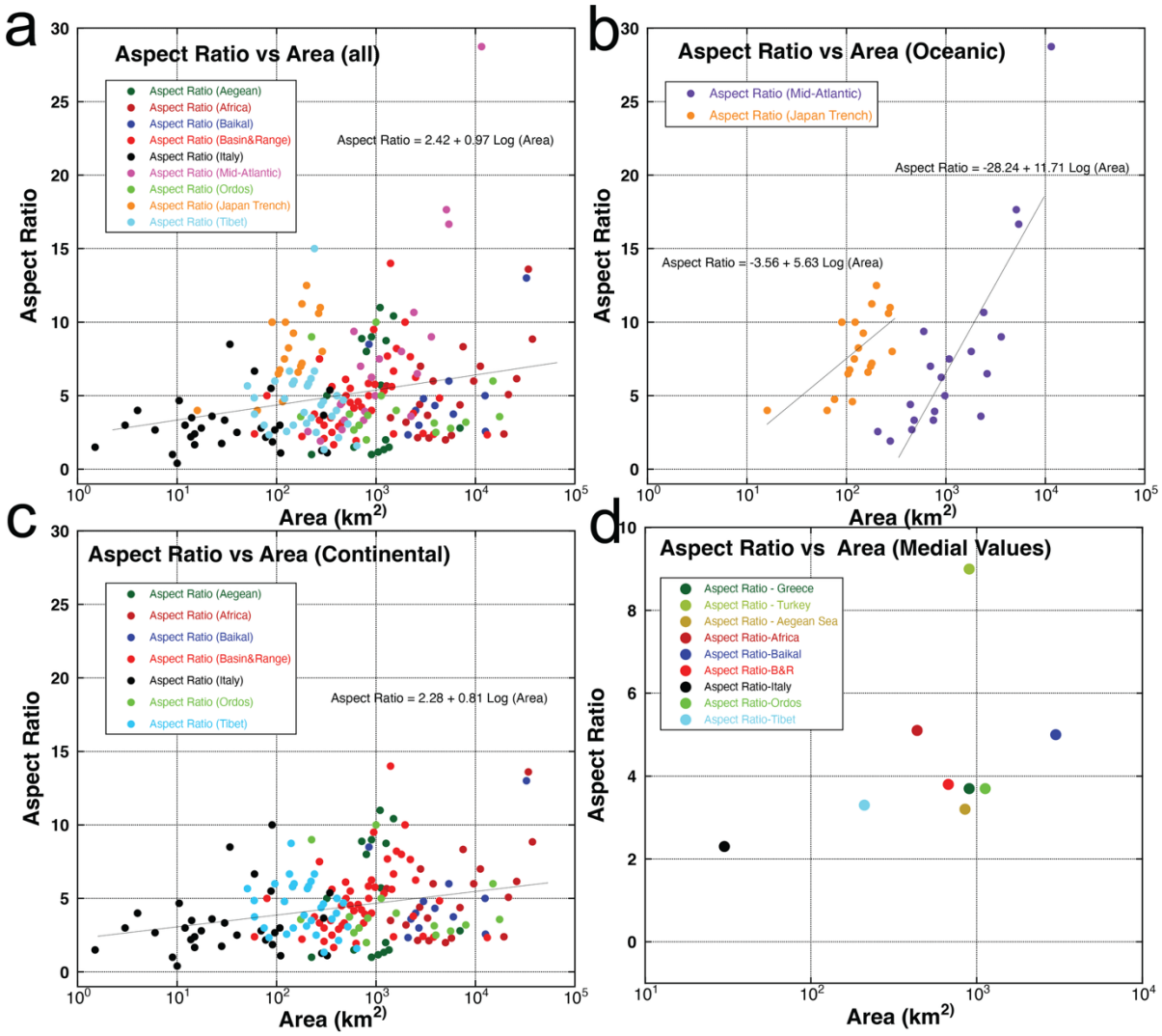

Figure 7 (a thru d). Aspect ratio versus basin area (a) for all basins, (b) for median values of each listed in Figures 5 and Figure 6a, respectively, (c) continental basins only, and (d) and oceanic basins only.

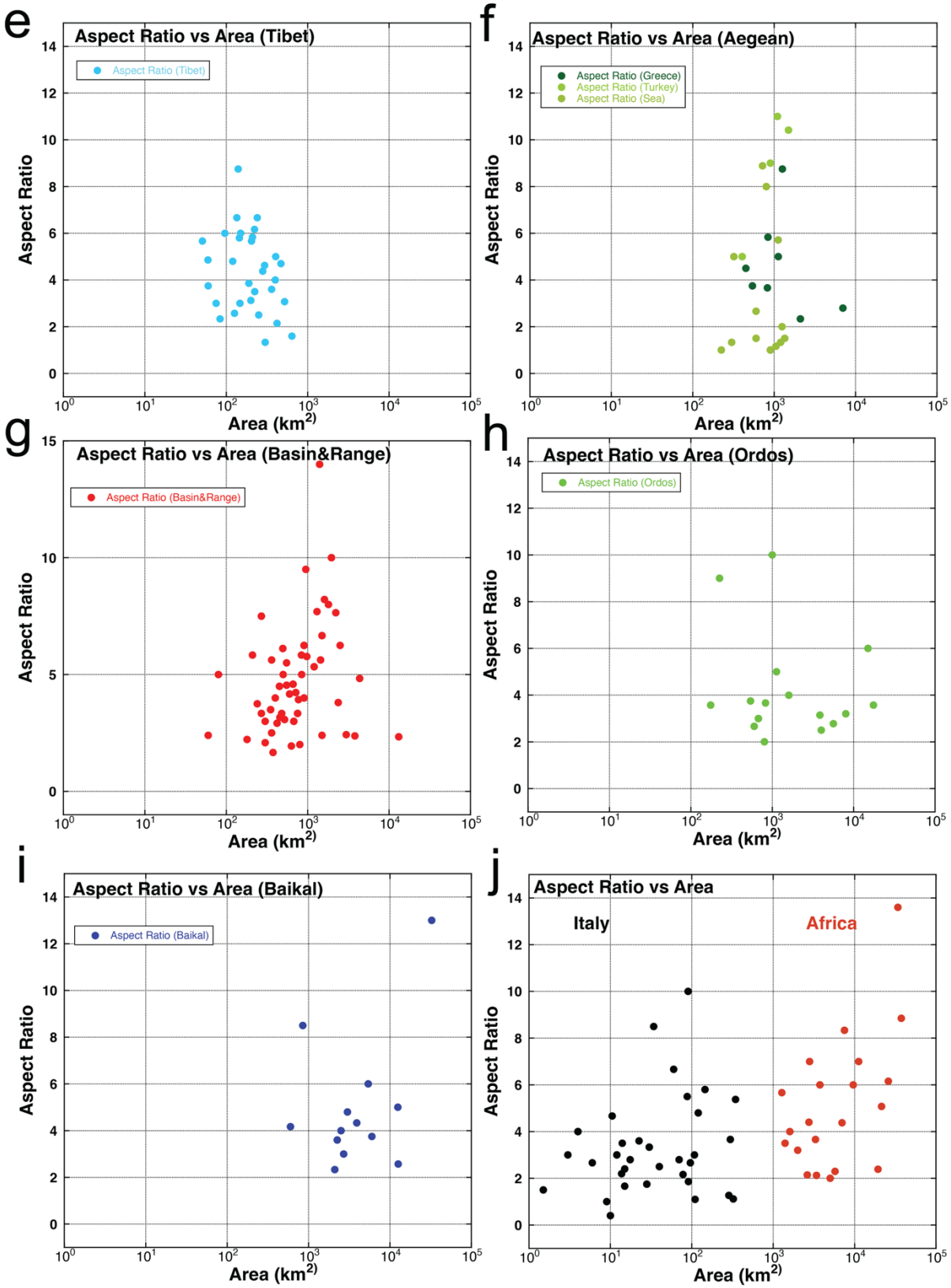

Figure 7 continued (e thru j). Aspect ratio versus basin areas in separate extensional regions of (e) Tibet, (f) the Aegean Sea, (g) the Basin and Range, (h) Ordos, (i) Baikal area, (j) Italy and Africa.

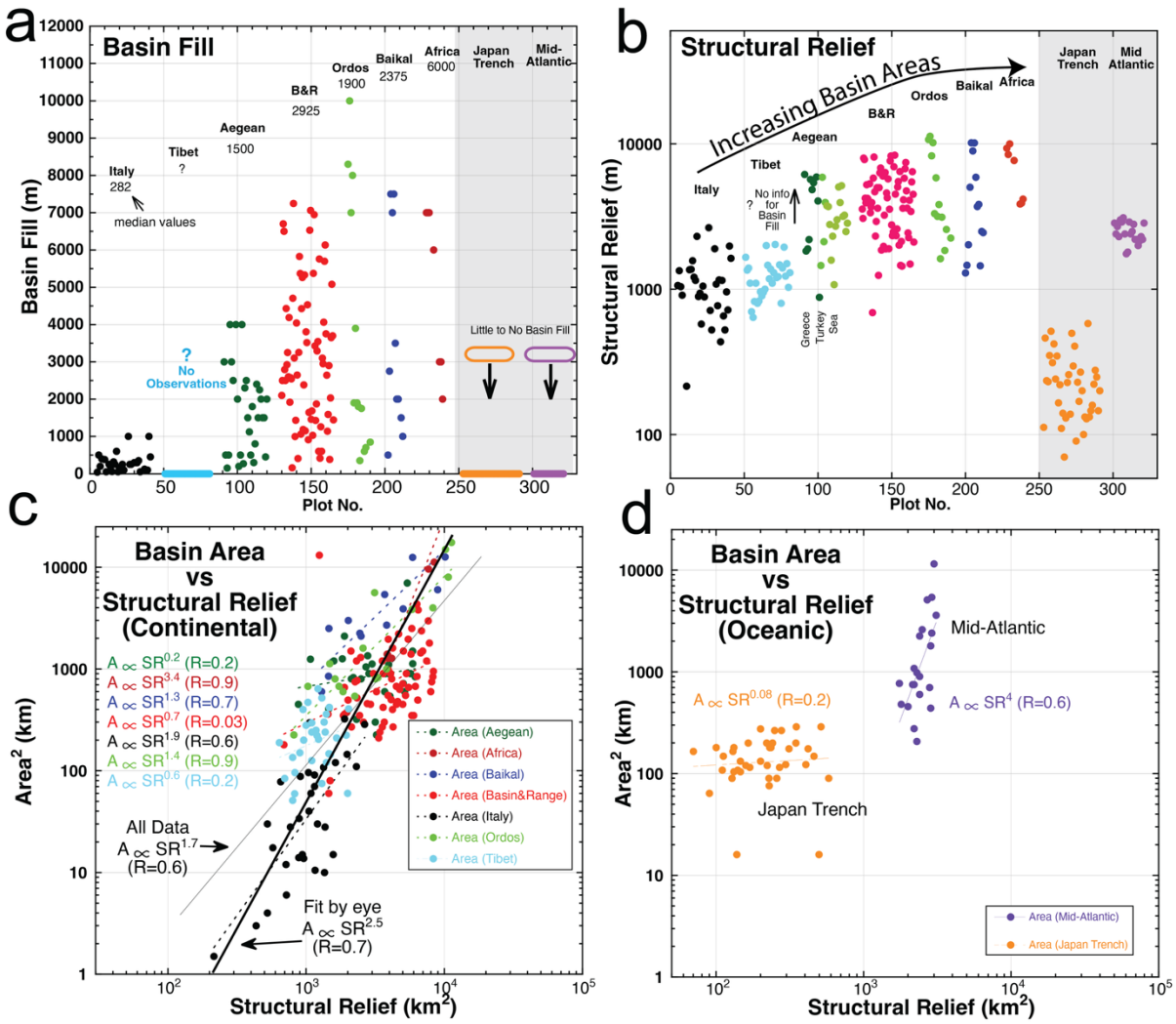

Figure 8. (a) Basin fill, (b) structural relief, and (c) and (d) basin area versus structural relief for basins in continents and oceans. respectively.

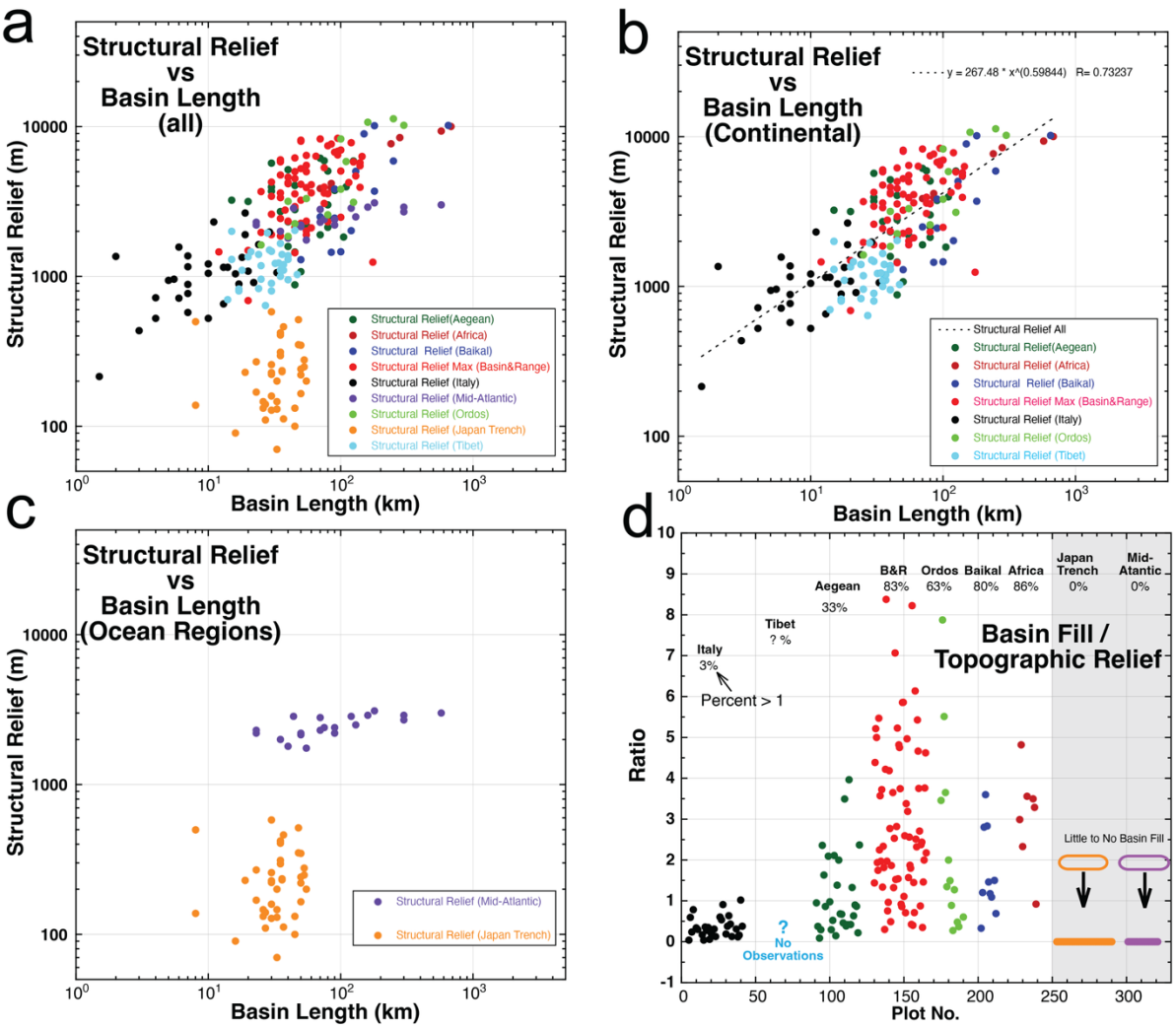

Figure 9. Structural relief versus basin length for (a) all basins, (b) continental basins, (c) marine basins. (d) Ratios of basin fill depths to adjacent maximum mountain heights. Ratios >1 indicate basin fill is major contributor to structural relief and ratios <1 occur in those basins where topographic relief is the primary contributor to the structural relief.

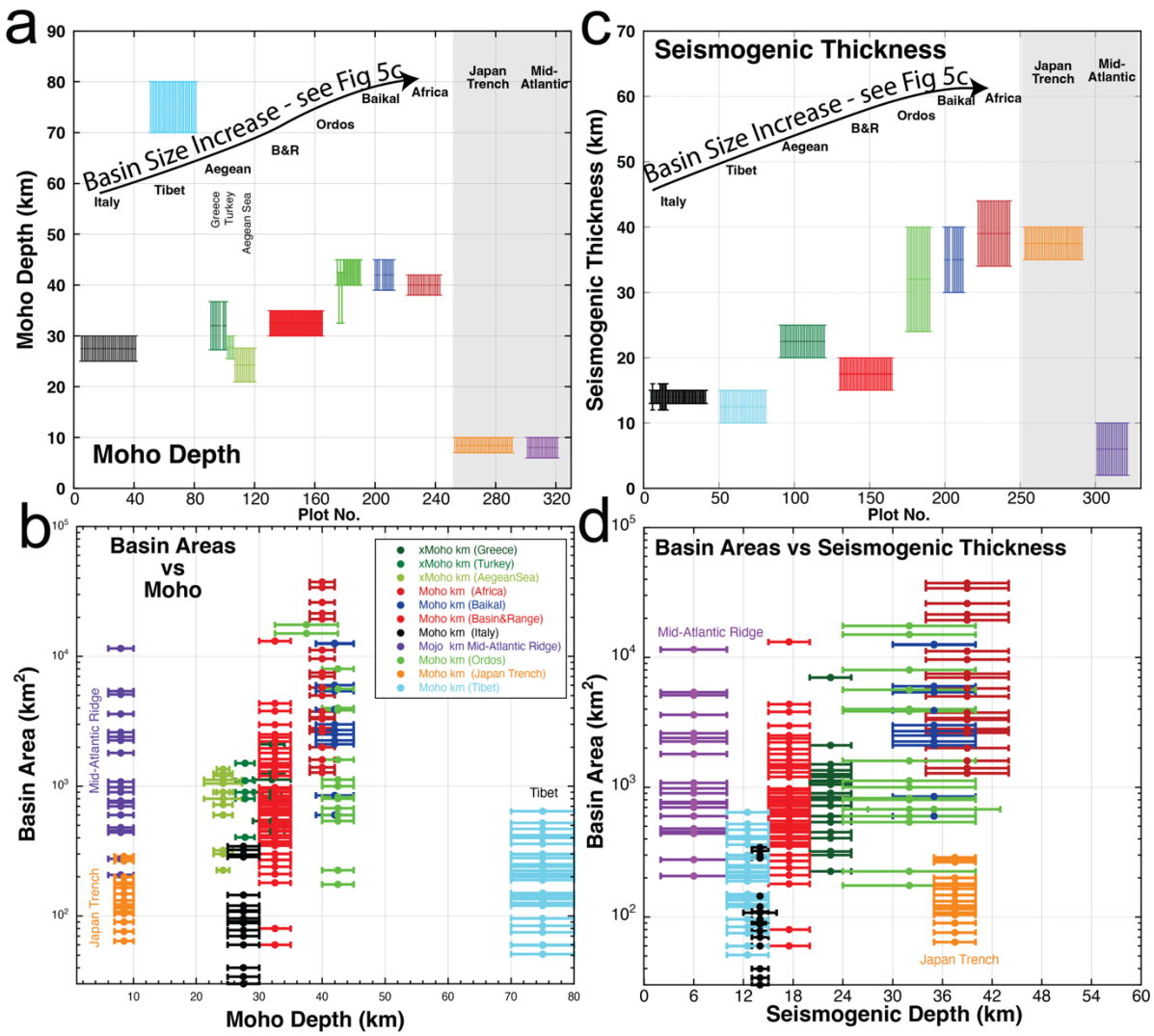

Figure 10. (a) Moho depth and (b) seismogenic thickness versus plot number. Basin area versus (c) Moho depth and (d) seismogenic thickness.

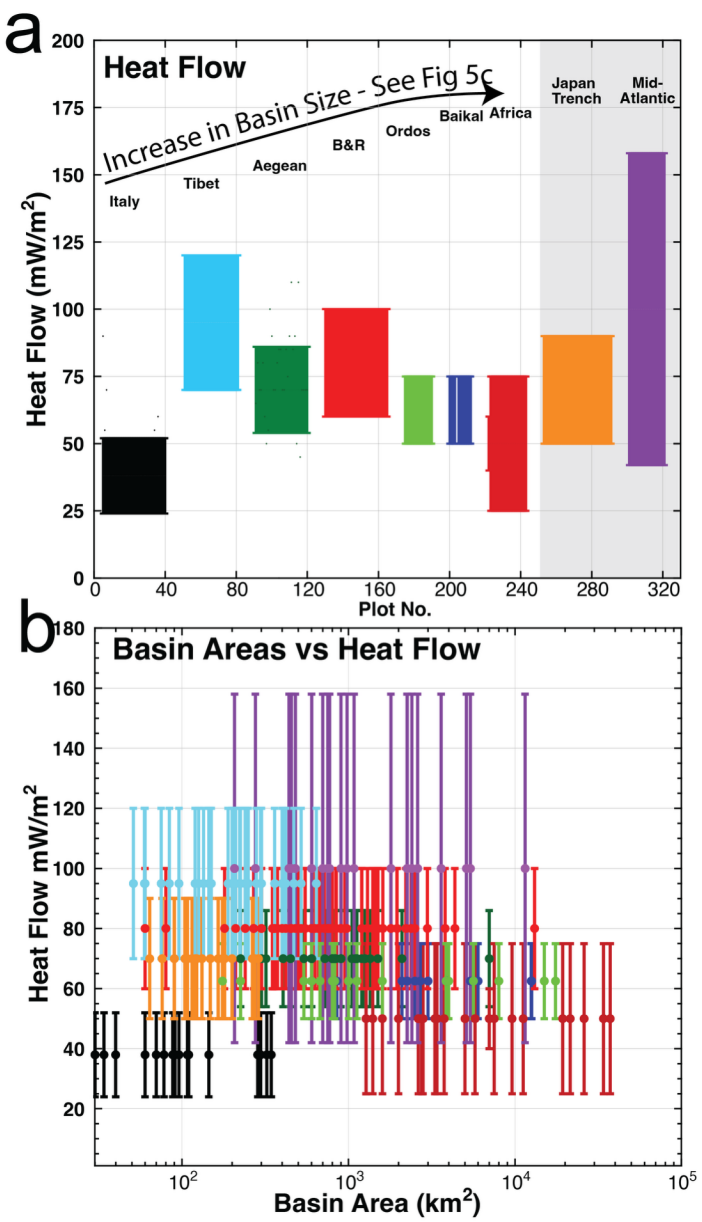

Figure 11. Heat flow plotted versus (a) plot number (b) and basin area.

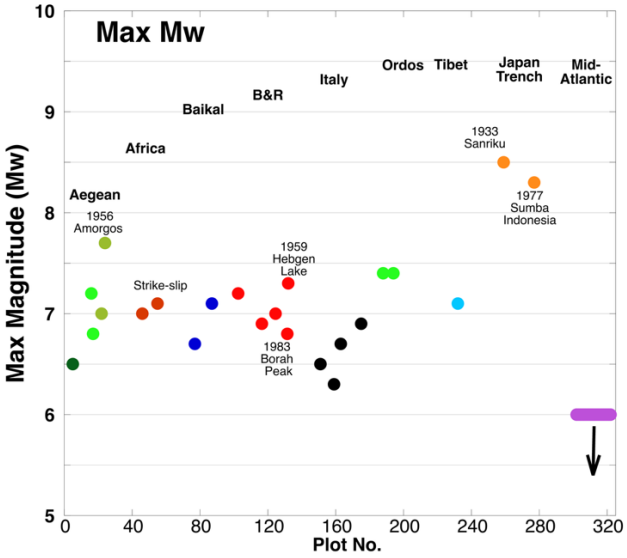

Figure 12. Moment magnitude Mw values for largest instrumentally recorded normal fault earthquakes in the different extensional regime versus plot number and basin area. The 1959 and 1983 earthquakes and the 1977 Sumba earthquakes occur in the Basin and Range and along the outer rise of a subducting plate, but outside of the regions in **Figure 2**.

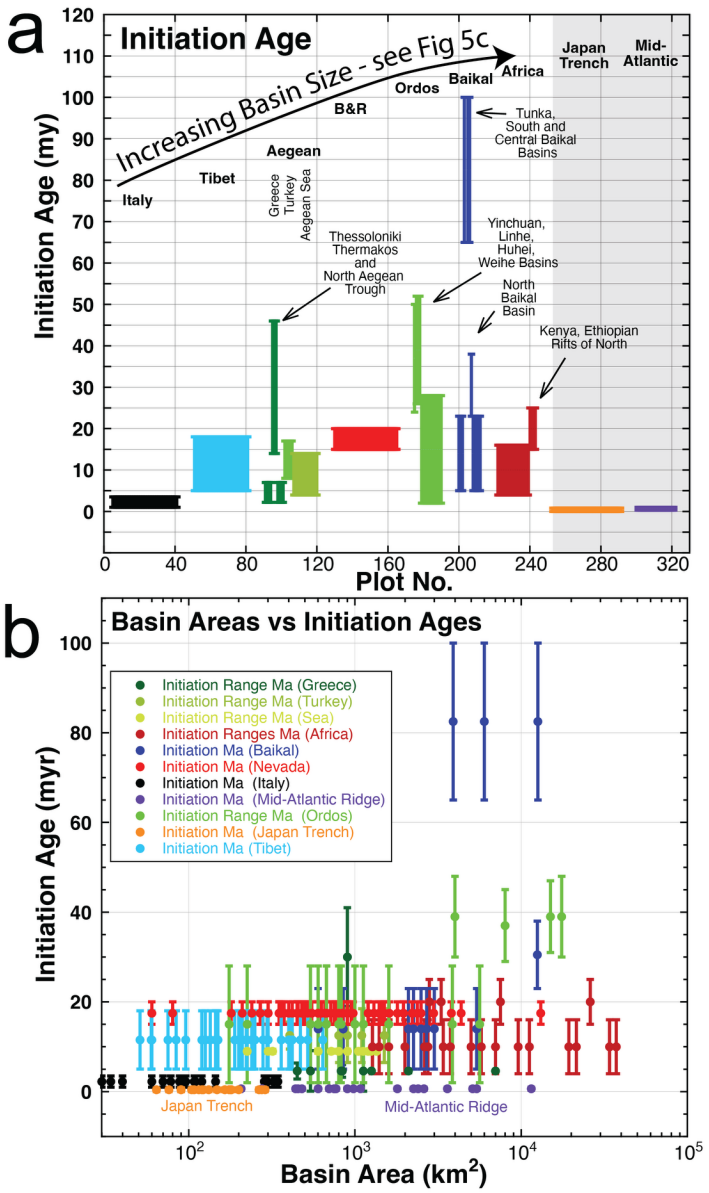

Figure 13. (a) Age active extension initiated and (b) Age active extension initiated in region versus individual basin areas.

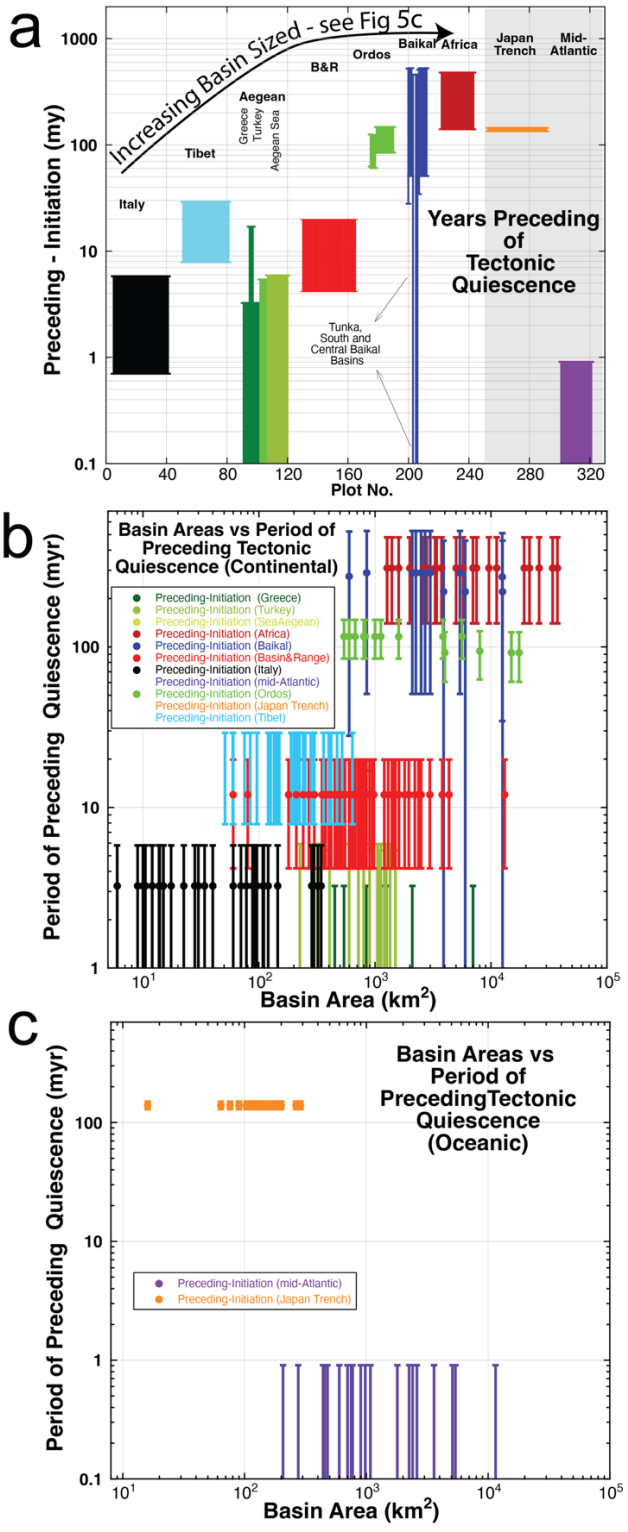

Figure 14. (a) Periods of tectonic quiescence preceding initiation of current extensional regimes versus (a) plot number and individual basin areas in (b) continental and (c) oceanic areas.

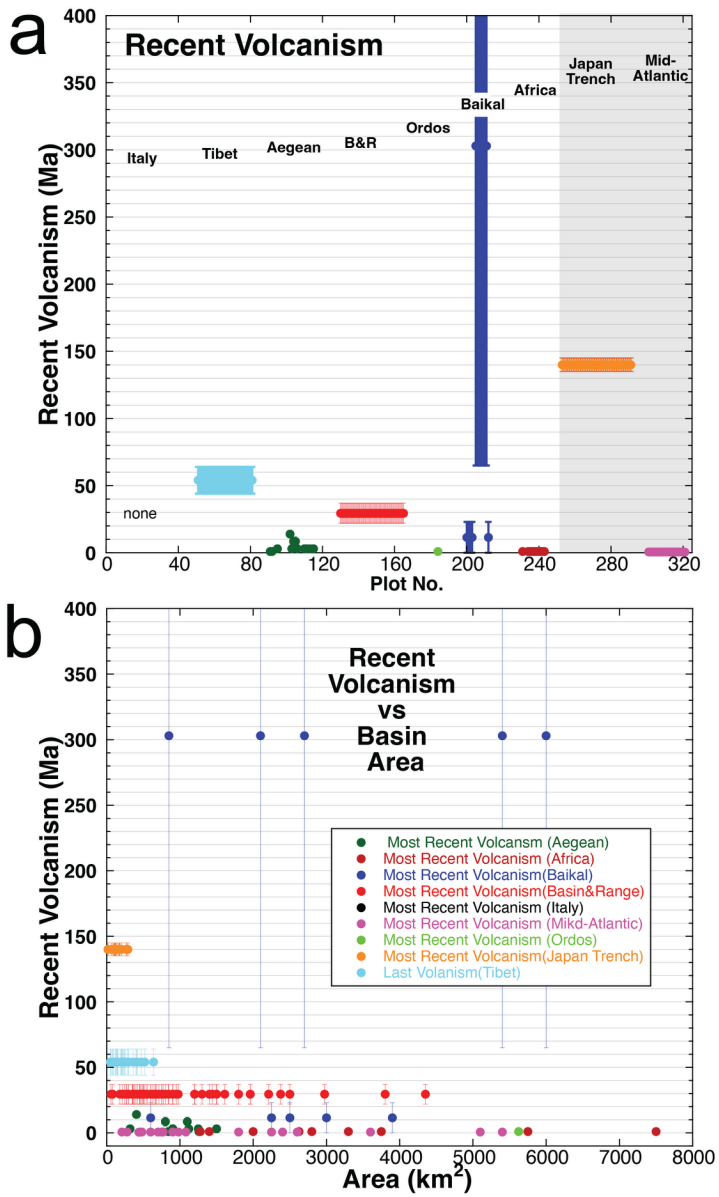

Figure 15. (a) Ages of most recent volcanism versus (a) plot number and (b) individual basin areas. Figure not capable of displaying spatial extent of volcanism. Regions of similar basin size show diverse ages of recent volcanism, precluding any systematics between volcanism and basin size.

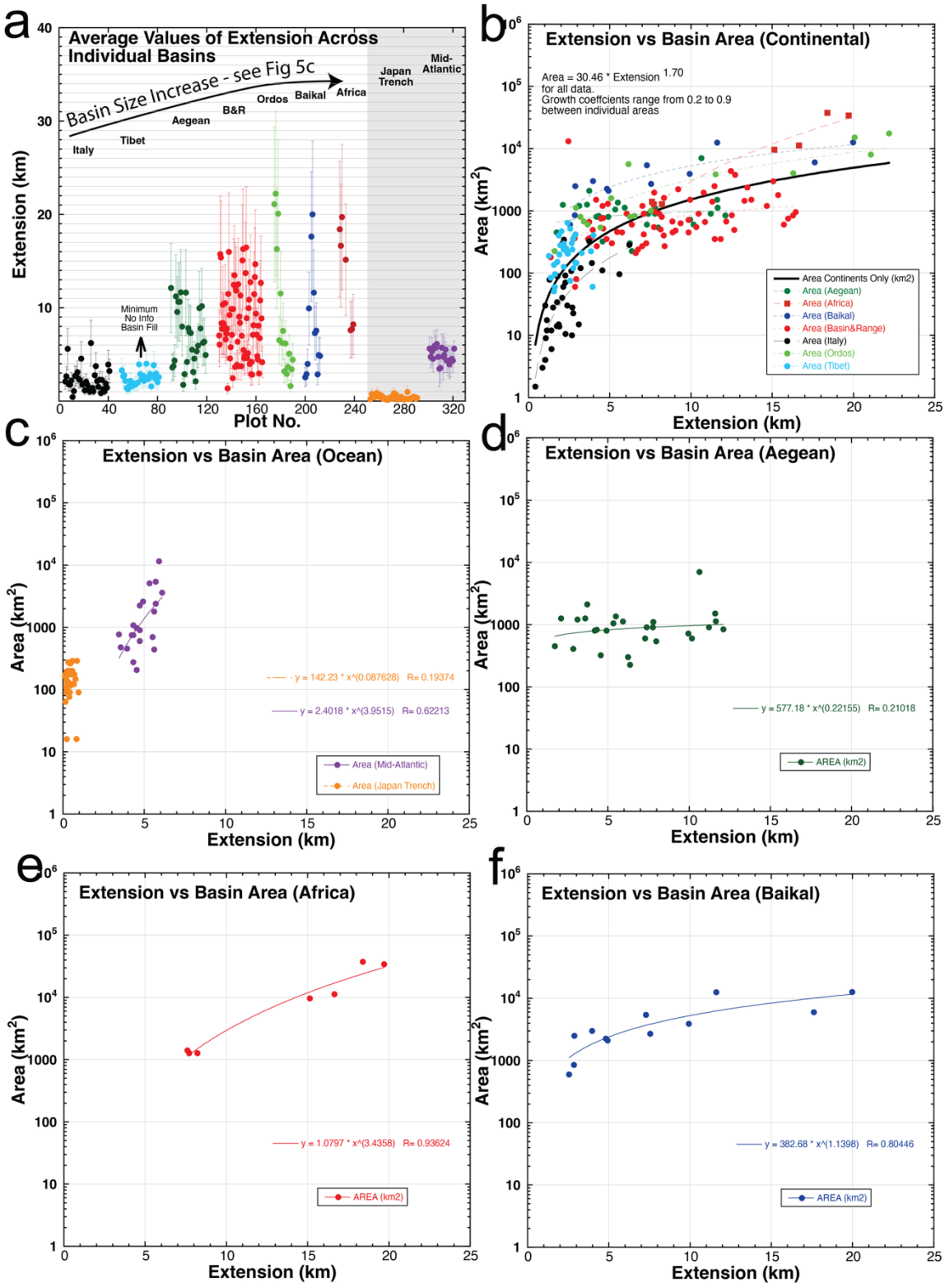

Figure 16 a to f. (See full caption after Figure 16j)

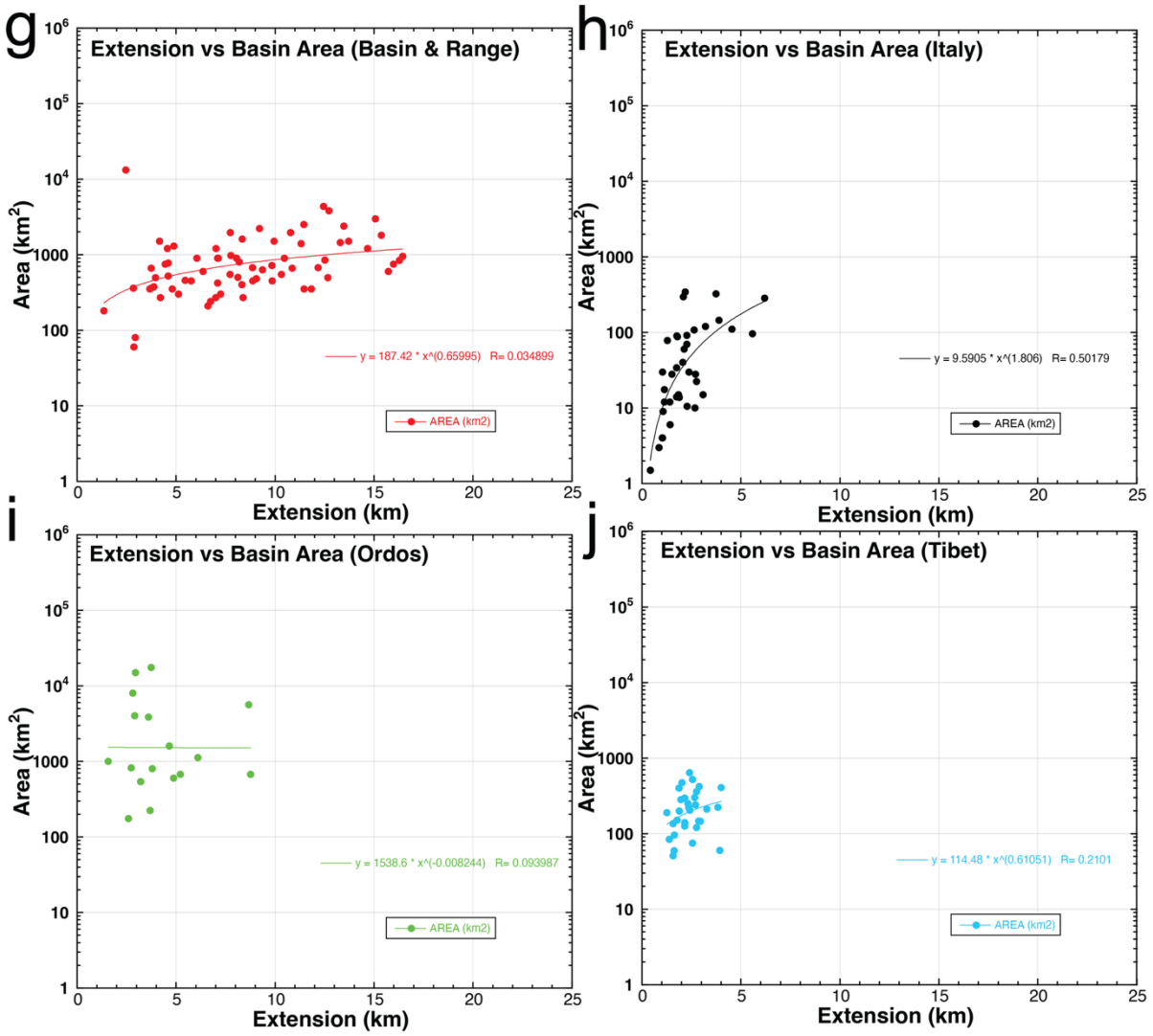

Figure 16. (a) Extensions of individual basins assuming 50°-70° dip. (b) Estimates of Extension versus areas of respective continental basins are plotted for (b) continental and (c) oceanic regions (d) Aegean, (e) Africa, (f) Baikal, (g) Basin and Range, (h) Italy, (i) Ordos, and (j) Tibet areas. Regression lines for visual reference. See text for discussion.

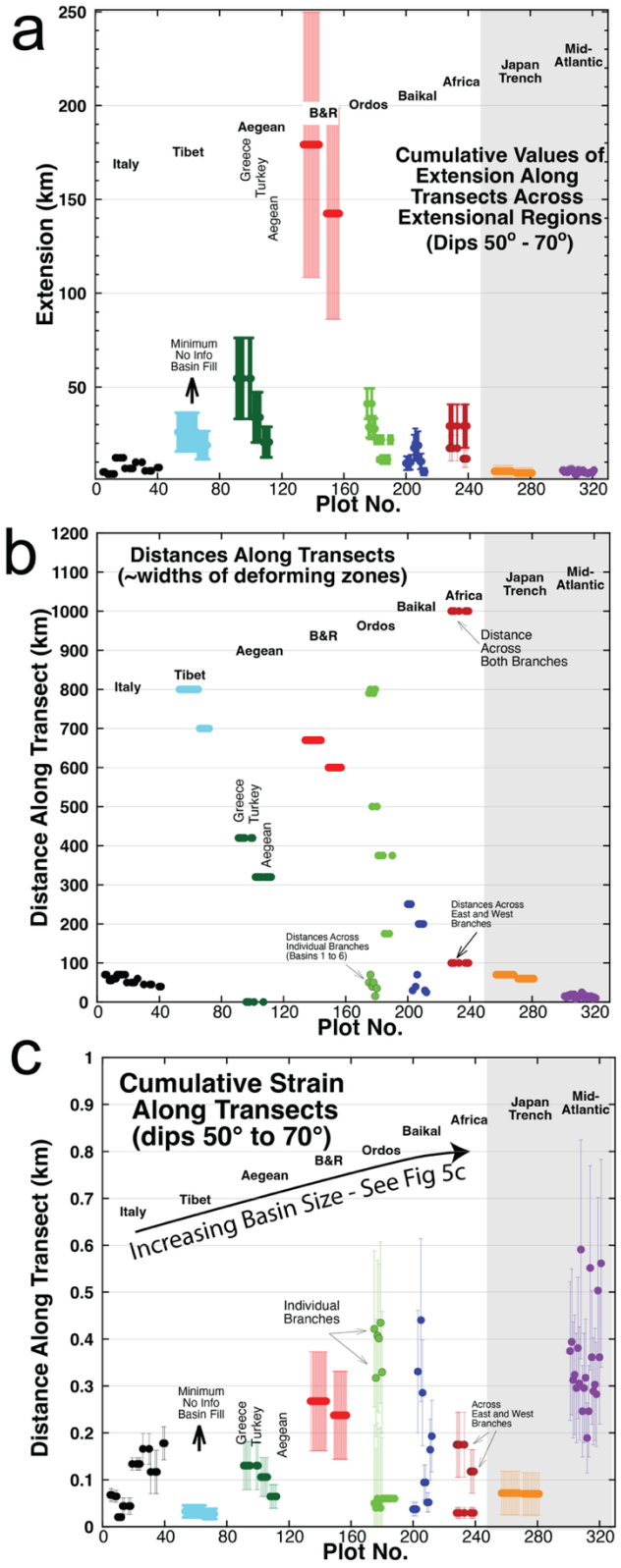

Figure 17. (a) Cumulative extension along transects across regions of extensional faulting, (b) the length of transects which are an approximate proxy of the width of the extending regions, and (c) the cumulative strain estimated by division of (a) by (b).

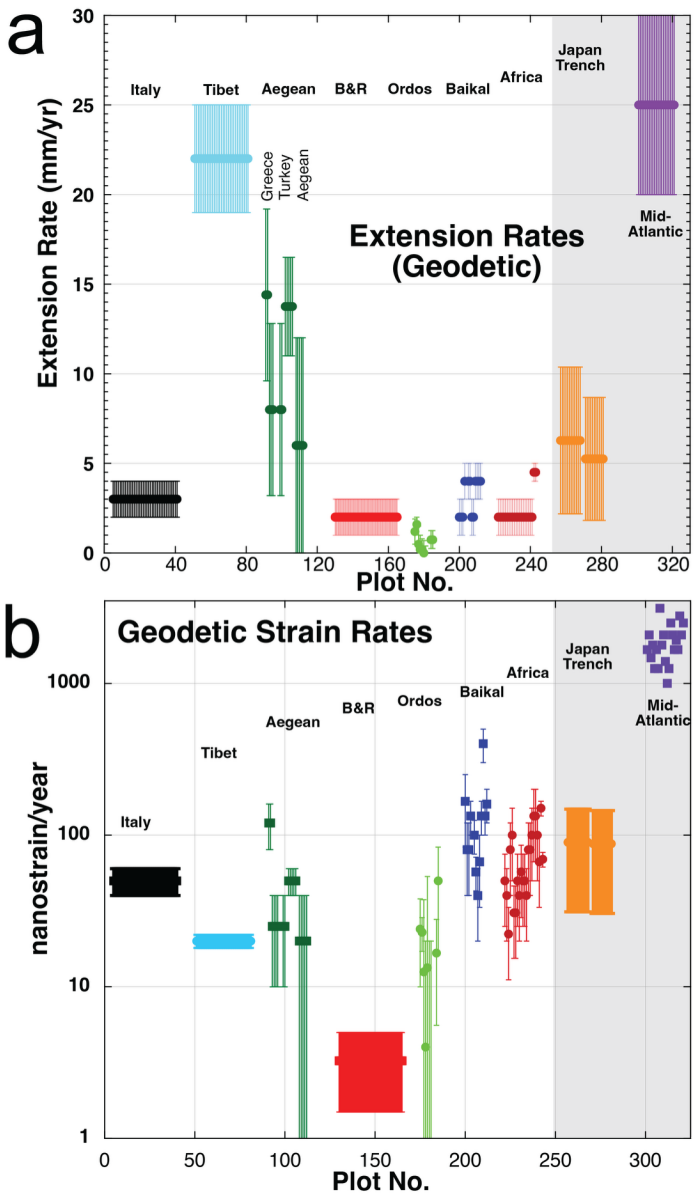

Figure 18. Geodetic rates of (a) extension and (b) extensional strain versus plot number.

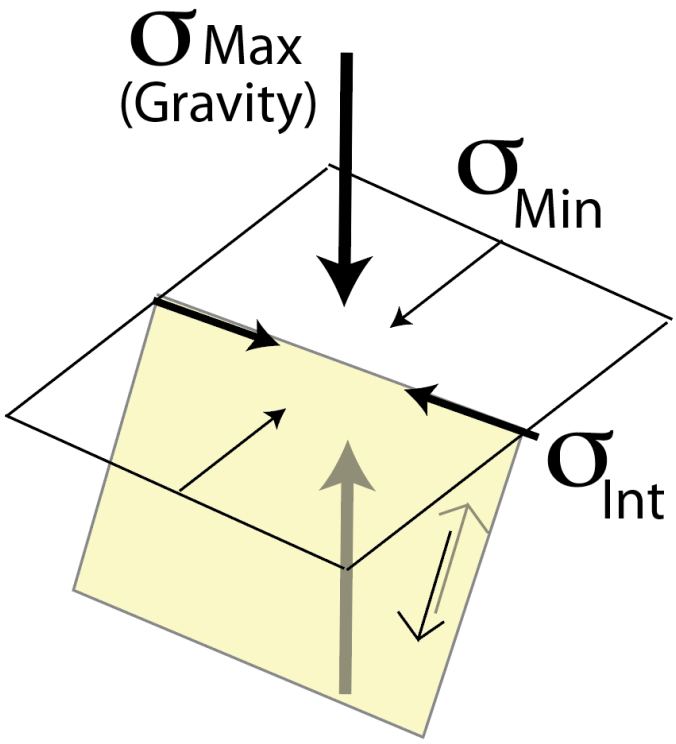

Figure 19. Crustal stresses σ are described by 3 principal axes: the maximum, minimum, and intermediate, generally oriented either perpendicular or parallel to the earths surface (e.g., Anderson, 1905; 1951. The vertical stress is attributed to gravity and the horizontal stresses to lithostatic load and tectonics. Normal faulting and crustal extension are limited to regions where where the vertical stress due to gravity is maximum.

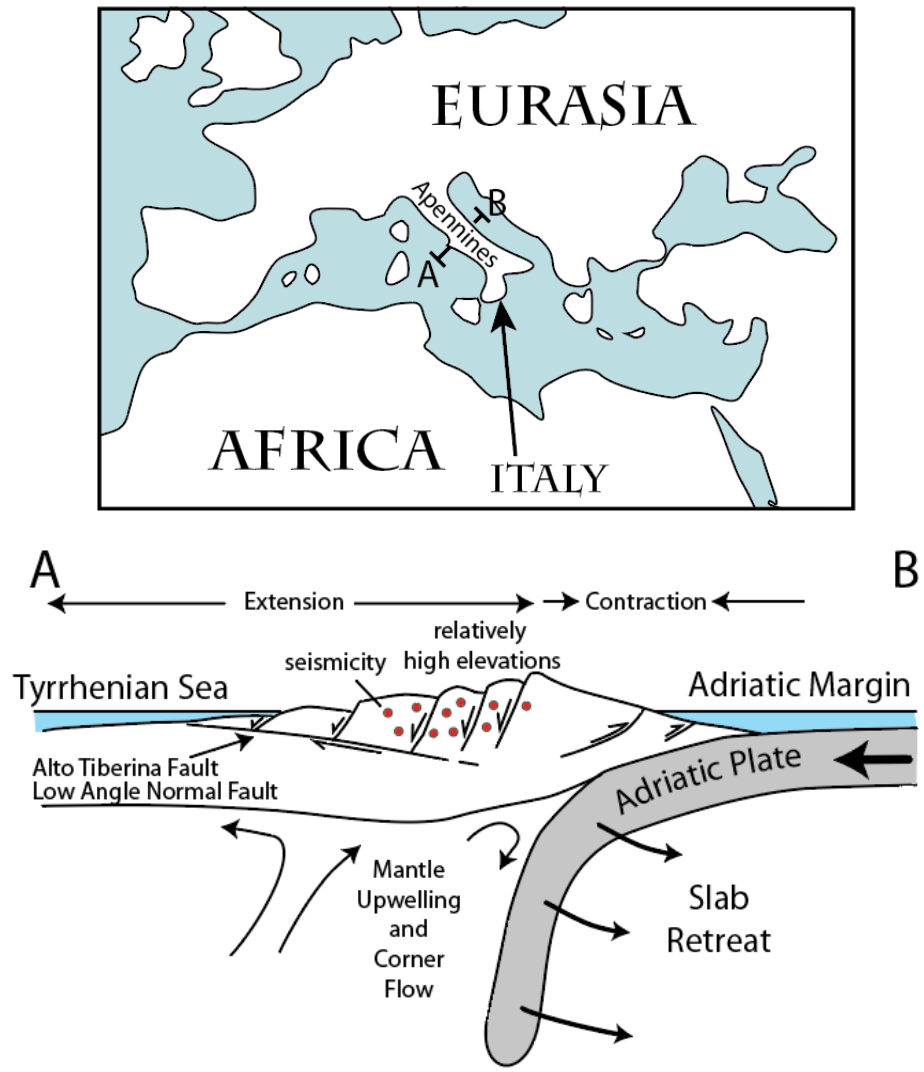

Figure 20. (upper) Location of Apennines in Italy and (lower) schematic cross-section illustrating factors that play role in presence of normal faulting and crustal extension in the Apennines (adapted from multiple sources, among them Cavinato and De Celles (1999), Chiaraluce et al. (2007) Chiarabba et al. (2005) and Lavecchia (2024).

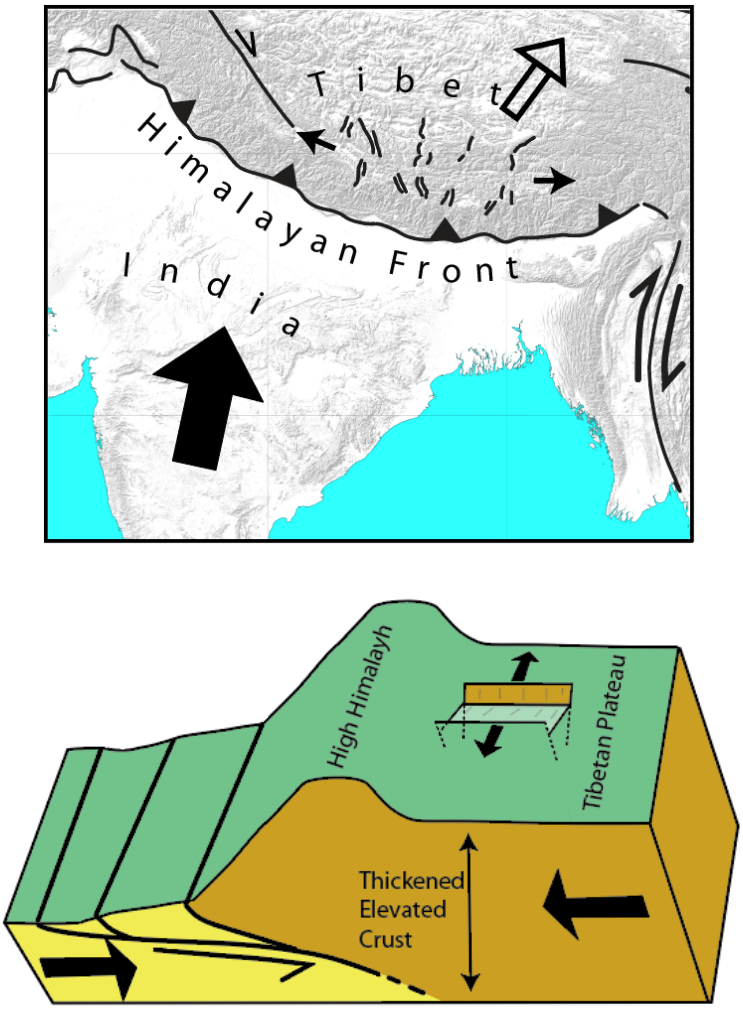

Figure 21. (upper) Tibetan normal faults and associated basins are generally oriented near perpendicular to the Himalayan fault and manifestation of east oriented crustal extension. (lower) Sketch illustrating explanations that attribute extension and Tibetan basin development to gravitational collapse resulting from extreme thickening of continental crust and increased elevation that accompanies northward impingement of India (yellow) into Tibet.

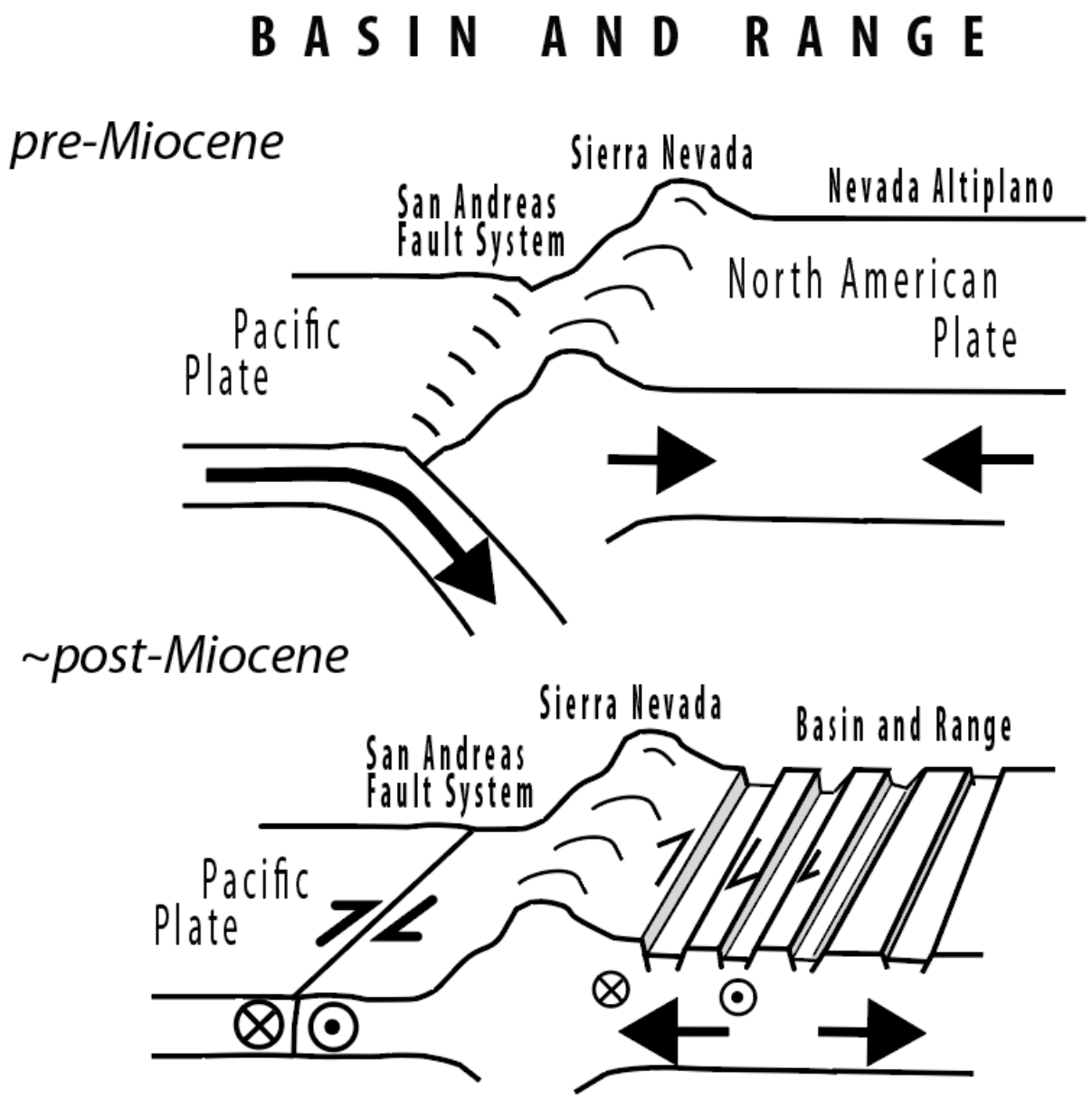

Figure 22. Transition of Pacific-North American plate boundary from subduction to strike slip in early Miocene time is commonly cited as responsible for development of the Basin and Range that is now described by a combination of strike-slip and normal fault motions.

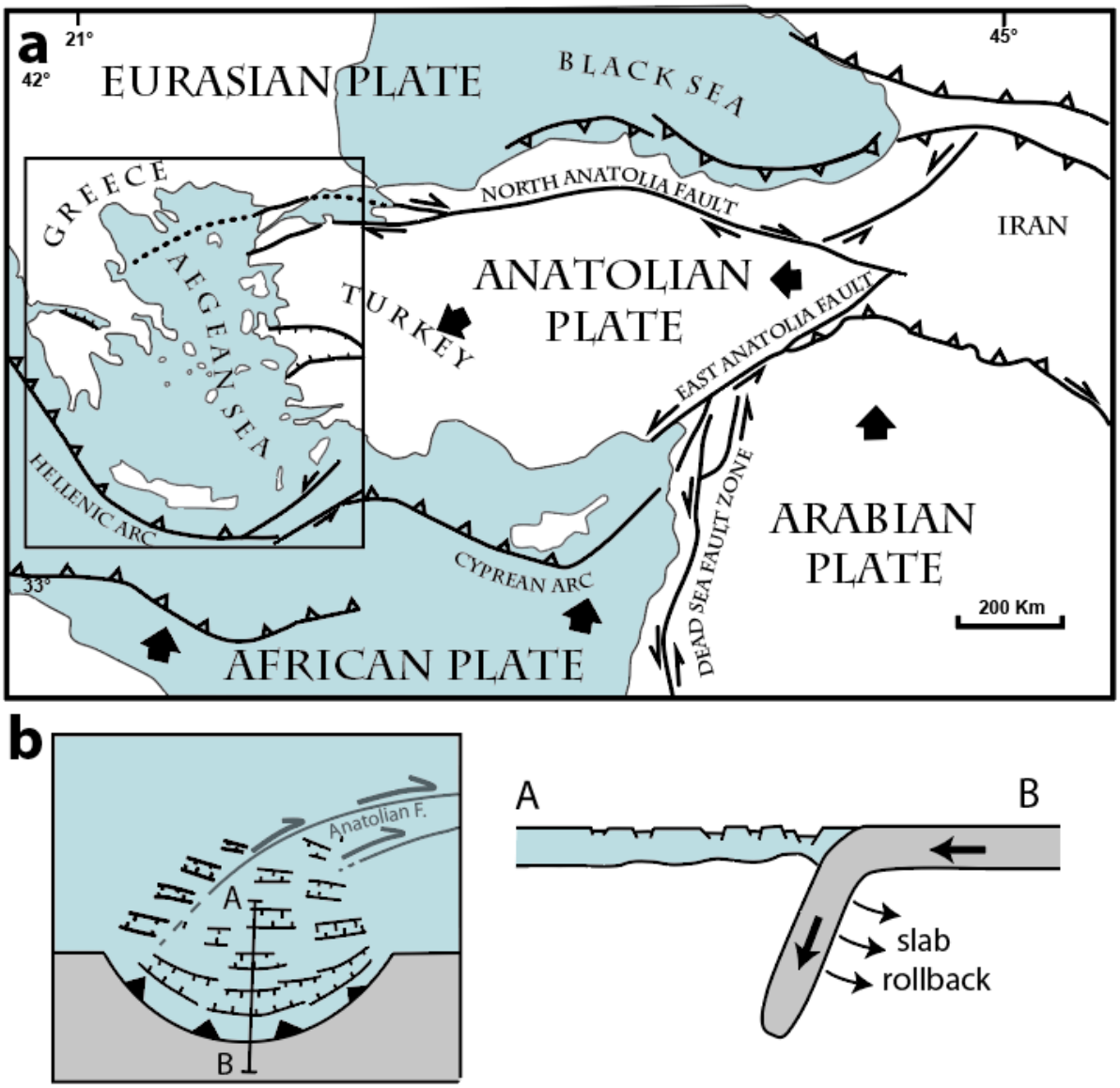

Figure 23. (a) Aegean Sea in regional tectonic framework and (b) sketches illustrating tectonic processes of back-arc extension due to slab rollback and right-lateral slip of Anatolia fault that contribute to ongoing extension.

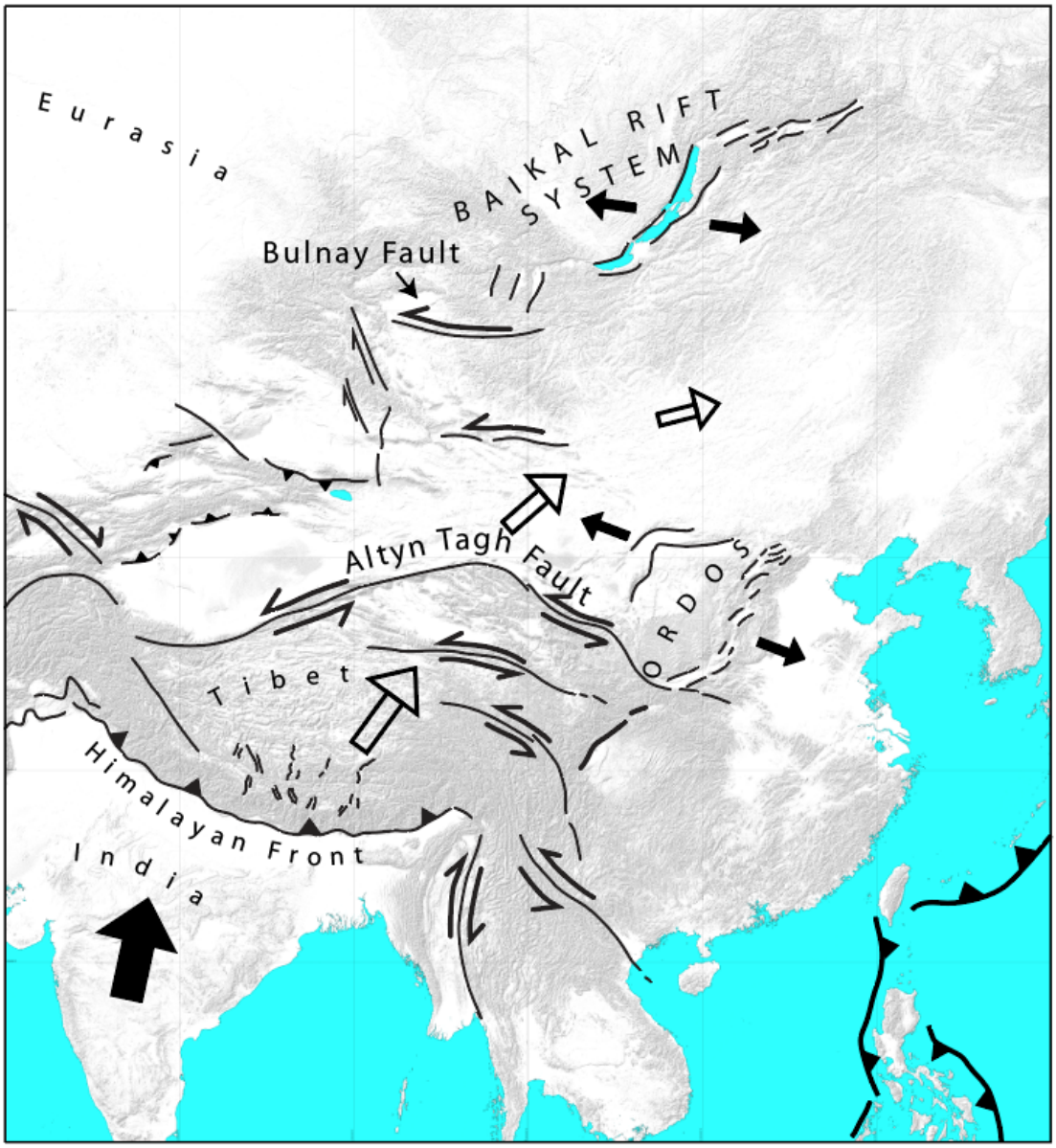

Figure 24. Deformation at the ends of major left-lateral faults that accommodate ongoing collision of India into Eurasia is the general explanation for the development of extensional basins around the Ordos plateau and along the Baikal Rift systems.

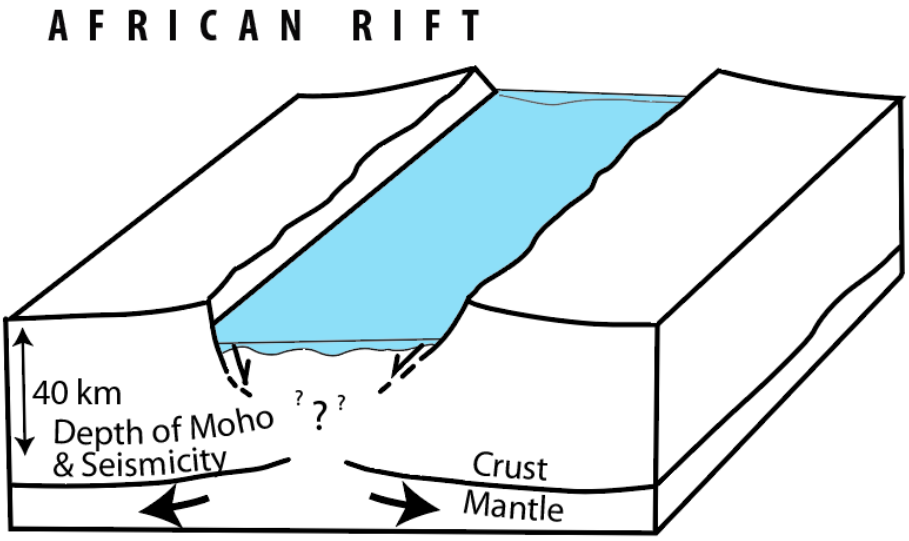

Figure 25. Simplified sketch of extension across East African Rift system driven by plate tectonic motions and mantle flow below a thick crust.

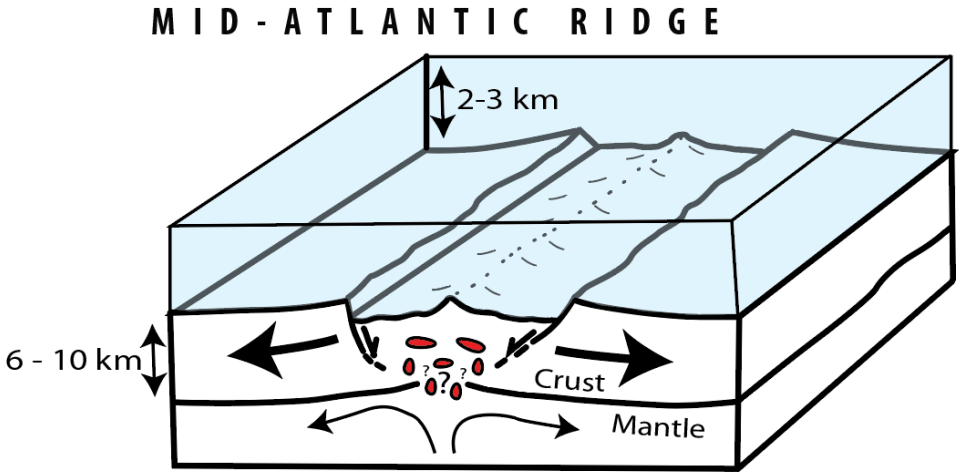

Figure 26. Simplified sketch emphasizes that extension at the ridge occurs with both magma accretion and faulting that result from horizontal plate tectonic motions accompanied by mantle flow.

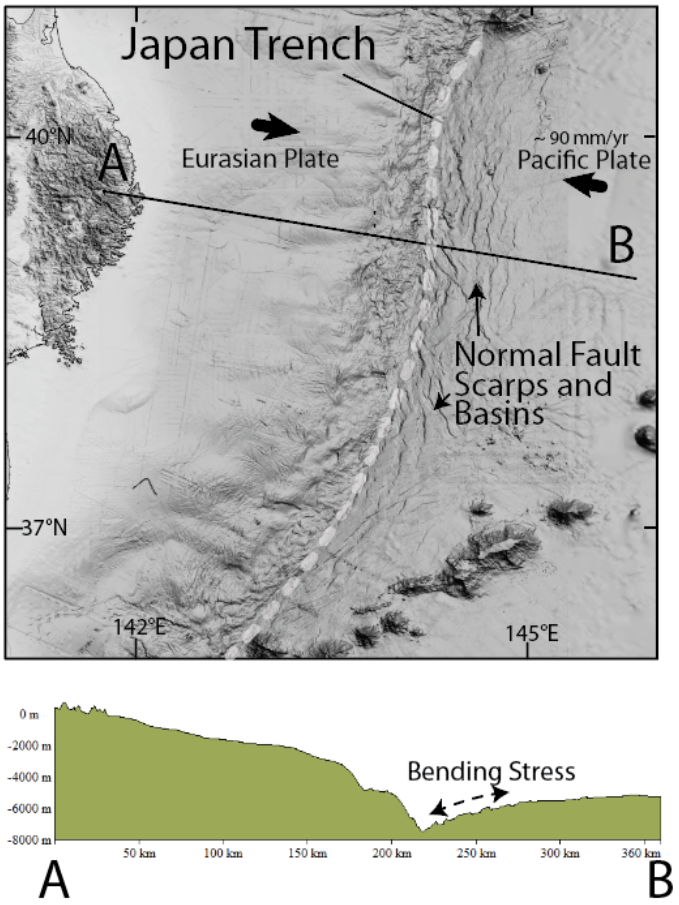

Figure 27. Digital elevation model and topographic cross section across Japan Trench outlined in **Figure 1**. Normal fault basins east of Japan Trench on Pacific Plate are attributed to bending stresses as Pacific Plate subducts beneath Eurasian Plate. Digital elevation model from GEBCO (2024).

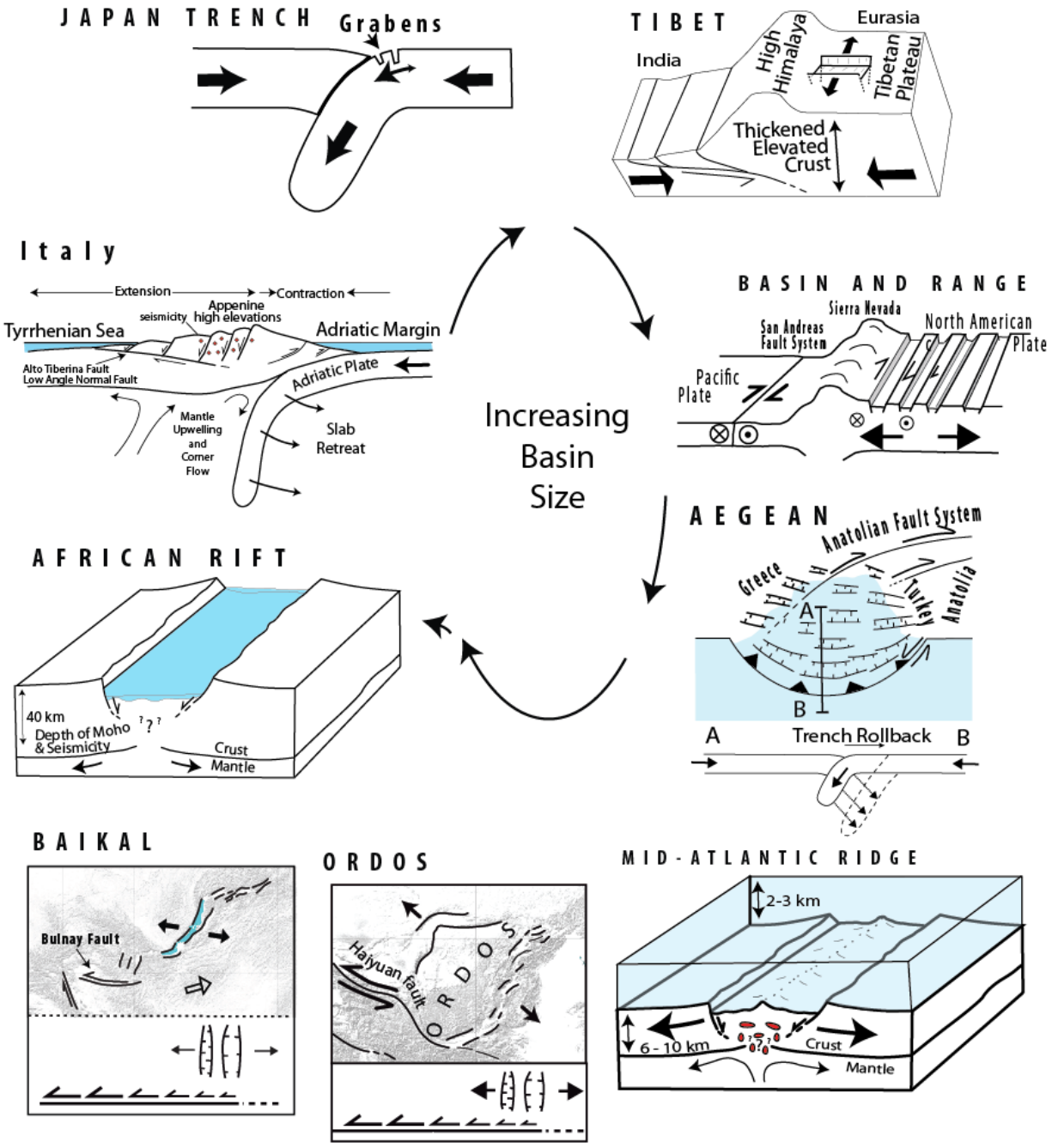

Figure 28. Regions of extension ordered in sequence of increasing basin areas that distinguish the regions, as documented and shown in **Figure 5**.